Digital repeat photography for phenological research in forest ecosystems

Oliver Sonnentag [a,b,*], Koen Hufkens [c], Cory Teshera-Sterne [a], Adam M. Young [d], Mark Friedl [c], Bobby H. Braswell [e], Thomas Milliman [e], John O'Keefe [f], Andrew D. Richardson [a]

[a] Harvard University, Department of Organismic and Evolutionary Biology, Harvard University Herbaria, 22 Divinity Avenue, Cambridge, MA 02138, USA
[b] Université de Montréal, Département de Géographie, Pavillon 520, 520, chemin de la Côte-Ste-Catherine, Montreal, QC H2 V 2B8, Canada
[c] Boston University, Department of Geography and Environment, 675 Commonwealth Avenue, Boston, MA 02215, USA
[d] State University of New York, College of Environmental Science and Forestry, 106 Bray Hall, 1 Forestry Drive, Syracuse, NY 13210, USA
[e] University of New Hampshire, Complex Systems Research Center, Morse Hall, 39 College Road, Durham, NH 08324, USA
[f] Harvard University, Harvard Forest, 324 North Main Street, Petersham, MA 01366, USA

ABSTRACT

Digital repeat photography has the potential to become an important long-term data source for phenological research given its advantages in terms of logistics, continuity, consistency and objectivity over traditional assessments of vegetation status by human observers. Red-green-blue (*RGB*) color channel information from digital images can be separately extracted as digital numbers, and subsequently summarized through color indices such as *excess green* ($ExG = 2G − [R + B]$) or through nonlinear transforms to chromatic coordinates or other color spaces. Previous studies have demonstrated the use of *ExG* and the green chromatic coordinate ($g_{cc} = G/[R + G + B]$) from digital landscape image archives for tracking canopy development but several methodological questions remained unanswered. These include the effects of diurnal, seasonal and weather-related changes in scene illumination on *ExG* and g_{cc}, and digital camera and image file format choice.

We show that g_{cc} is generally more effective than *ExG* in suppressing the effects of changes in scene illumination. To further reduce these effects we propose a moving window approach that assigns the 90th percentile of all daytime values within a three-day window to the center day (*per90*), resulting in three-day *ExG* and g_{cc}. Using image archives from eleven forest sites in North America, we demonstrate that *per90* is able to further reduce unwanted variability in *ExG* and g_{cc} due to changes in scene illumination compared to previously used mean mid-day values of *ExG* and g_{cc}.

Comparison of eleven different digital cameras at Harvard Forest (autumn 2010) indicates that camera and image file format choice might be of secondary importance for phenological research: with the exception of inexpensive indoor webcams, autumn patterns of changes in g_{cc} and *ExG* from images in common JPEG image file format were in good agreement, especially toward the end of senescence. Due to its greater effectiveness in suppressing changes in scene illumination, especially in combination with *per90*, we advocate the use of g_{cc} for phenological research. Our results indicate that g_{cc} from different digital cameras can be used for comparing the timing of key phenological events (e.g., complete leaf coloring) across sites. However, differences in how specific cameras "see" the forest canopy may obscure subtle phenological changes that could be detectable if a common protocol was implemented across sites.

1. Introduction

The importance of phenological research for understanding the consequences of global environmental change on vegetation is indisputable (Morisette et al., 2009). Phenological research requires long-term (years to decades) observations of vegetation status across plant species and various temporal and spatial scales. To overcome the limitations of field observations by individuals (e.g., logistics and lack of consistency, continuity and objectivity) for species-level vegetation monitoring, several "near-surface" remote sensing approaches have been proposed (Garrity et al., 2010; Richardson et al., 2007; Ryu et al., 2010).

Recently, conventional digital cameras taking repeated images of the landscape at high frequencies (several images per day) over several months or even years have obtained increased attention for phenological research (Ahrends et al., 2009; Graham et al., 2010;

Ide and Oguma, 2010; Kurc and Benton, 2010; Migliavacca et al., 2011; Richardson et al., 2009a; Sonnentag et al., 2011). Typically, these digital cameras are mounted on instrumentation towers or installed at look-outs and vantage points, resulting in horizontal or oblique views of vegetation canopies. The obtained images represent combined brightness levels from three color channels spanning overlapping wavelength ranges of the visible part of the electromagnetic spectrum. Thus, near-infrared (NIR) information useful for studying vegetation (Tucker, 1979) is generally lacking with most conventional digital cameras unless the cameras are modified to leverage the NIR sensitivity of the imaging sensor. Using a large number of spatially distributed high-frequency archives of digital landscape images allows for detailed land surface characterization over time, which could then be used for remote sensing product evaluation and refinement (Graham et al., 2010; Jacobs et al., 2009).

With a few exceptions (e.g., Sonnentag et al., 2011), most ecosystem-scale studies employing multi-month or -year archives of digital landscape images were conducted at sites where vegetation structure and thus the phenological cycles were not affected by human or animal activity (Ahrends et al., 2009; Richardson et al., 2007, 2009a). Examples include the broad-leaf temperate deciduous forests of Europe and North America. In these ecosystems increasing and decreasing canopy greenness might be indicative of the increasing and decreasing amount of photosynthetically active green leaves and their condition during spring and autumn, respectively. In most of these studies, daily values of canopy greenness as described by a color index (e.g., *excess green*) were linked to seasonal changes in net ecosystem carbon dioxide exchange, canopy photosynthesis, and other important biophysical measures (Ahrends et al., 2009; Richardson et al., 2007, 2009a).

Despite these first promising applications several important questions remained unanswered. For example, images taken over the course of a day for several months or years are subjected to scene illumination changes due to the daily rotation of the Earth (Ahrends et al., 2008; Richardson et al., 2009a), the Earth's revolution, cloudiness and other changes in atmospheric transmittance (i.e., overall weather) conditions. Consequently, the recorded brightness levels, usually in the red-green-blue (*RGB*) color space, are the integrated response to scene illumination as controlled by illumination and viewing geometries (digital camera orientation and viewing angle) and shadowing effects, time-of-day, day-of-year and weather conditions, in addition to canopy color changes due to plants' phenological cycle. Disentangling these different influences on *RGB* brightness levels is a complicated task, but understanding especially the role of scene illumination changes might help to minimize their influences on the resultant descriptors of canopy greenness.

One usually overlooked technical aspect is digital camera choice. Considering the large variety of digital cameras and image file formats (e.g., RAW, TIFF, JPEG), understanding the role of camera and image file format choice is fundamental for interpreting the resultant camera signal in a phenological framework. For example, are differences in imaging sensor technologies used by different cameras relevant for phenological research? Are digital images stored in unprocessed RAW format superior over images stored in a compressed, "lossy" format (e.g., JPEG)?

The goal of our study was to formulate a set of recommendations for the use of digital cameras to monitor canopy greenness in forest ecosystems based on high-frequency archives of digital landscape images. These recommendations are based on four objectives that together shed light on the influences of scene illumination changes, and camera and image file format choice on the seasonal dynamics of canopy greenness from digital landscape image archives, and on a discussion of different digital camera options for phenological research from an end-user perspective (i.e., financial and logistical constraints, infrastructure and maintenance requirements, user-friendliness, etc.).

Our first objective is to characterize diurnal and seasonal patterns of canopy greenness (e.g., *excess green* or the green chromatic coordinate) as influenced by diurnal (time-of-day), seasonal (day-of-year) and weather-related changes in scene illumination in images archives from a deciduous-dominated (Harvard Forest) and a coniferous-dominated forest site (Howland Forest). Our second objective is to propose a simple statistical methodology that minimizes the influence of changes in scene illumination on estimates of *excess green* or the green chromatic coordinate. We test this method using one-year image archives from Harvard Forest and Howland Forest and nine additional forest sites and one non-vegetated site. Our third objective is to compare image archives from different digital cameras overlooking the same portion of the forest canopy at Harvard Forest to identify camera types and/or models that are useful for phenological research. Our fourth objective is to examine differences in mean diurnal patterns of canopy greenness between digital images in RAW and JPEG format.

2. Background

2.1. Scene illumination and color indices

In addition to visual inspection of combined image brightness levels as true colors, the color channel information of digital images can be extracted as separate *RGB* digital numbers (*DN*) for quantitative analysis. However, it needs to be stressed that the *RGB* color space is less suited for the quantitative analysis of true color due to the high correlation among the three *RGB* color space components (Cheng et al., 2001).

Red-green-blue brightness levels are influenced by scene illumination, but these influences can be suppressed by a nonlinear transform of *RGB DN* to *rgb* chromatic coordinates (Gillespie et al., 1987; Woebbecke et al., 1995), defined as:

$$r_{cc} = \frac{R}{(R+G+B)}; \quad g_{cc} = \frac{G}{(R+G+B)}; \quad b_{cc} = \frac{B}{(R+G+B)} \tag{1}$$

In contrast to *RGB* brightness levels, *rgb* chromatic coordinates describe the actual three primary colors red, green and blue as perceived by human vision.

Over the last two decades, numerous color indices for digital images have been formulated and explored especially in the agricultural literature (Adamsen et al., 1999, 2000; Meyer and Neto, 2008; Perez et al., 2000; Woebbecke et al., 1995). Based on manually taken nadir images of individual plants, the goal of many of these studies was improved distinction between green plants and soil/residue background prior to binarization (Meyer and Neto, 2008; Perez et al., 2000; Woebbecke et al., 1995). A widely used example to describe canopy greenness is *excess green* (*ExG*) defined as:

$$2G - (R+B) \tag{2}$$

Excess green was found to be superior over other color indices for the distinction between green plants and soil/residue background by enhancing the signal from green plant material (Woebbecke et al., 1995). Similar to the *rgb* chromatic coordinates, *ExG* is also able to minimize the effects of changes in scene illumination. The value ranges of *ExG* and the *rgb* chromatic coordinates are driven strongly by the imaging sensor (e.g., bit depth, color balance), thus the direct comparison of their absolute values from different digital cameras remains difficult.

2.2. Digital camera technology

A range of different techniques exist for digital repeat photography (also called time-lapse photography), including digital cameras directly addressable via Internet Protocol (herein referred to as 'webcams'), game and plant cameras ('game-cams' and 'plant-cams'; the most basic digital cameras specially marketed at hobbyists with interests in wildlife and gardening), and consumer-grade digital point-and-shoot (P-and-S), digital bridge or digital single-lens reflex (DSLR) cameras in combination with an intervalometer. These digital camera options differ widely in terms of complexity, the imaging sensor used, resolution and light sensitivity (i.e., a digital camera's ISO setting), infrastructure (e.g., networking), maintenance and, ultimately, costs. Obviously, conventional, off-the-shelf digital camera options are not calibrated scientific instruments. Consequently, many digital image archives, initiated for different monitoring purposes (e.g., security, visibility, tourism and recreation), exist, but their widespread scientific application is challenging due to the wide variety of resulting image qualities and resolutions.

The central component of digital cameras is the imaging sensor, typically based on traditional charged-coupled device (CCD), complementary metal-oxide-semiconductor (CMOS) technology, Junction Field Effect Transistor (JFET), or the more recent Live MOS technology. Essentially, all imaging sensor technologies consist of silicon chips with a two-dimensional array of photosites to record scene brightness levels for three color channels across overlapping *RGB* wavelengths (i.e., over the primary colors of the visible portion of the electromagnetic spectrum). The brightness of a scene is determined by illumination intensity (outdoors: direct vs. diffuse sunlight) and the spectral characteristics of the materials contained in the scene. The recorded *RGB* brightness levels are quantized as discrete digital numbers, *DN*, which, together with additional information from the image acquisition process (i.e., pre-exposure settings such as ISO, aperture, shutter speed, focus), are captured in a raw, unprocessed format (RAW). A recent review of digital camera technology and image file formats is given by Verhoeven (2010).

The most common standard of file formats for digital images was defined by the Joint Photographic Experts Group (JPEG). Compared to other common image file formats such as the Tagged Image File Format (TIFF), the JPEG standard encompasses "lossy" compression algorithms, i.e., when saving an image based on this standard, image size is reduced at the cost of information loss. In addition, the JPEG standard also includes rarely used "lossless" compression algorithms and both the "lossy" and lossless algorithms of the newer JPEG2000 standard were developed for improved compression performance (http://www.jpeg.org/). However, most webcams, game- and plant-cams, and consumer-grade P-and-S digital cameras output digital images in either TIFF or original "lossy" JPEG standard-based image file formats, generated by conversion from the unprocessed image in RAW format by the digital camera. As part of this conversion process a set of pre-defined digital camera settings (e.g., white balance, contrast, sharpness, etc.) are applied to the unprocessed digital images, leaving only limited options for post-processing. In contrast, more sophisticated digital cameras such as most DSLRs provide the option to output images as RAW files, thus providing maximum information content and post-processing options. However, the internal processing of digital cameras is often proprietary and reverse engineering of a particular RAW format is basically impossible.

Regardless of the image file format, each true color in a digital image can be represented by some combination of *RGB DN* as conceptualized in the Cartesian *RGB* color space. Ultimately, the maximum total number of possible true colors in the *RGB* color space depends on the bit depth of the imaging sensor. For example, an image in JPEG format with 8-bit quantization per color channel results in 0–255 brightness levels for each primary color and thus over 16 million possible true colors.

3. Methods

3.1. Study sites

To characterize the influence of diurnal, seasonal and weather-related changes in scene illumination our initial focus was on one-year archives of digital landscape images from deciduous-dominated Harvard Forest and coniferous-dominated Howland Forest. We used nine additional one-year archives from different deciduous- (six sites) and coniferous-dominated (three sites) forest sites and from one non-vegetated site to test our proposed statistical methodology to calculate *ExG* and g_{cc}. We used eleven additional three-month archives from Harvard Forest to examine the role of digital camera and image file format choice. Eleven of the resulting twelve sites were located in the United States and one site, Chibougamou, was located in Canada.

With one exception (Arbutus Lake), all sites are established research or long-term monitoring sites associated with AmeriFlux (http://public.ornl.gov/ameriflux/), the Canadian Carbon Program (http://www.fluxnet-canada.ca/), the USDA Forest Service Air Resource Management program (http://www.fs.fed.us/air/index.htm) or the National Park Service Air Resources program. All sites are part of the PhenoCam network (http://phenocam.unh.edu), a recent initiative to continuously monitor phenology at ecosystem scale with image archives of digital landscape images across the US and adjacent Canada (Richardson et al., 2007, 2009a).

Detailed site descriptions are provided elsewhere and in Table 1. In brief, five of the sites are located in the Midwest (Morgan Monroe State Forest) and New England regions (Arbutus Lake; Bartlett Forest; Harvard Forest Environmental Measurement Site (EMS); Howland Forest) of the United States, and an adjacent region in Canada (Chibougamau) at low to moderate elevations (<400 m asl), thus in temporal and boreal climate zones of the Northern Hemisphere (Table 1). In contrast, six of the sites are located in various mountainous regions of the United States (the Cascades: Pasayten Wilderness; the Appalachians: Dolly Sods Wilderness, Shining Rock Wilderness, Smoky Purchase-Knob; the Rocky Mountains: Niwot Ridge; the Colorado Plateau: Grand Canyon) at higher elevations (>1200 m asl). Together, the eleven forest sites represent a variety of tree species characteristic of deciduous- and coniferous-dominated forest ecosystems in temperate, boreal, subalpine, and alpine climate zones. For comparison of *ExG* and g_{cc} over deciduous- and coniferous-dominated forest ecosystems, we included a one-year image archive from a non-vegetated site, semi-arid Grand Canyon, for which we did not expect the measured signal to vary seasonally.

3.2. Digital cameras

3.2.1. Scene illumination changes and statistical methodology

Within the PhenoCam network, different digital cameras are employed to take repeated landscape images at different intervals, resolutions, viewing geometries, and in some cases for different purposes (Table 2). Specific models from Axis' (http://www.axis.com) and StarDot's (http://www.stardot-tech.com/) suite of indoor/outdoor webcams were installed for phenological research at AmeriFlux forest sites (Bartlett Forest; Chibougamau; Harvard Forest EMS; Howland Forest; Morgan Monroe State Forest) and at Arbutus Lake based on positive initial experiences and also for purposes of network continuity (Richardson et al., 2007, 2009a). Images from these digital cameras were taken at high frequencies (every 30 min between 04:00 and 21:30 local time, except for Bartlett Forest), transferred via FTP (push) and stored on the PhenoCam server.

Table 1
PhenoCam forest study sites (Decid. = deciduous-dominated; Conif. = coniferous-dominated).

Site	Lat.; long. (d.d.)	Elev. (m asl)	Forest type	Dominant tree species	Year	Reference
Arbutus Lake	43.98; −74.23	535	Decid.	Sugar maple (*Acer saccharum*); American beech (*Fagus grandifolia*)	2009	http://www.esf.edu/hss/em/huntington/arbutusCam.html
Bartlett Forest[a]	44.06; −71.29	268	Decid.	Red maple (*Acer rubrum*); American beech	2009	Richardson et al. (2007)
Chibougamou[b]	49.69; −74.34	380	Conif.	Black spruce (*Picea mariana*)	2009	Bergeron et al. (2007)
Dolly Sods Wilderness[c]	39.11; −79.43	1141	Decid.	Sugar maple; red maple; American beech	2009	http://www.fsvisimages.com/
Grand Canyon[d]	36.06; −112.12	2177	–	–	2009	http://www.nature.nps.gov/air/WebCams/
Harvard Forest Environmental Measurement Site (EMS)[a]	42.54; −72.17	340	Decid.	Red oak (*Quercus rubra*); red maple; eastern hemlock (*Tsuga canadensis*)	2009	Urbanski et al. (2007)
Howland Forest[a]	45.20; −68.74	80	Conif.	Red spruce (*Picea rubens*); eastern hemlock; red maple; balsam fir (*Abies balsamea*)	2009	Hollinger et al. (2004)
Morgan Monroe State Forest[a]	39.32; −86.41	275	Decid.	Sugar maple; tulip poplar (*Liriodendron tulipifera*)	2009	Schmid et al. (2000)
Niwot Ridge[b]	40.033; −105.55	3050	Conif.	Subalpine fir (*Abies lasiocarpa*); Engelman spruce (*Picea engelmannii*); lodgepole pine (*Pinus contorta*)	2009	Monson et al. (2002)
Pasayten Wilderness[c]	48.39; −119.90	1250	Conif.	Ponderosa pine (*Pinus ponderosa*)	2009	http://www.fsvisimages.com/
Smoky Purchase-Knob[d]	35.59; −83.08	1550	Decid.	Yellow birch (*Betula alleghaniensis*); American beech; red maple; tulip poplar	2009	http://www.nature.nps.gov/air/WebCams/
Shining Rock Wilderness[c]	35.39; −82.77	1500	Decid.	Yellow birch; American beech; red maple; tulip poplar	2008	http://www.fsvisimages.com/

[a] AmeriFlux.
[b] Canadian Carbon Program.
[c] USDA Forest Service Air Resource Management program.
[d] National Park Service Air Resources program.

Table 2
Digital camera overview (n.s. = not specified; n.s.f. = not specified further): intervals are ten minutes (10-min), half-hourly (hh) or hourly (h); imaging sensors are CCD or CMOS in inch-type format (except for the Pentax K100D and Olympus E-420); types are outdoor (out.) or indoor (in.) webcam, plant-cam, game-cam, digital single-lens reflex camera (DSLR), or consumer-grade digital point-and-shoot camera (P-and-S).

Site	Manufacturer; model	Interval; temporal coverage (h local time)	Imaging sensor	Resolution	Type	View direction; tilt angle from horizontal (0°)	Reference
Arbutus Lake	StarDot; NetCam SC 1.3MP	hh; 04:00–21:30	1/2.5″-type CMOS	1296 × 960	Out. webcam	~N; ~20°	This study
Bartlett Forest	Axis; 211	10-min; 12:00–13:00	1/4″ CCD	640 × 480	Out. webcam	~N; ~20°	Richardson et al. (2009a)
Chibougamou	StarDot; NetCam SC 1.3MP	hh; 04:00–21:30	CMOS (n. s. f.)	1296 × 960	Out. webcam	~NE; ~20°	This study
Dolly Sods Wilderness	Olympus; SP-500	3-h; 09:00–15:00	1/2.5″-type CCD	1599 × 1199	DSLR camera	~S, 0°	This study
Grand Canyon	Olympus; E-420	h; 08:00–20:00	Live MOS (n.s.f.)	640 × 480	DSLR camera	~N, 0°	This study
Harvard Forest Environmental Measurement Site (EMS)	StarDot; NetCam SC 1.3MP	hh; 04:00–21:30	1/2.5″-type CMOS	1296 × 960	Out. webcam	~N; ~20°	This study
Harvard Forest[b]	Axis; 207MW	hh; 05:00–21:30	1/3″-type CMOS	1280 × 720	In. webcam	~N; ~20°	This study
Harvard Forest[b]	Axis; 211	hh; 05:00–18:30	1/4″-type CCD	640 × 480	Out. webcam	~N; ~20°	Richardson et al. (2009a)
Harvard Forest[b]	Axis; 223M	hh; 05:00–21:30	1/2.7″-type CCD	1600 × 1200	Out. webcam	~N; ~20°	This study
Harvard Forest[b]	StarDot; NetCam SC 1.3MP	hh; 05:00–20:30	1/2.5″-type CMOS	1296 × 960	Out. webcam	~N; ~20°	This study
Harvard Forest[b]	StarDot; NetCam XL 3MP	hh; 05:00–19:30	1/2″-type CMOS	2048 × 1536	Out. webcam	~N; ~20°	Richardson et al. (2009a)
Harvard Forest[b]	Vivotek; IP7160	hh; 05:00–20:00	1/3.2″-type CMOS	1600 × 1200	Out. webcam	~N; ~20°	This study
Harvard Forest[b]	D-Link; DCS-920	hh; 05:00–20:30	1/4″-type CMOS	320 × 240	In. webcam	~N; ~20°	Sonnentag et al. (2011)
Harvard Forest[b]	Wingscapes; PlantCam WSCA04	hh; 00:00–24:00	n.s.[c]	2048 × 1536	Plant-cam	~N; 20°	This study
Harvard Forest[b]	Moultrie; Game Spy I-60	h; 00:00–24:00	n.s.[c]	2048 × 1536	Game-cam	~N; 20°	Kurc and Benton (2010)
Harvard Forest[b]	Pentax; K100D[a]	hh; 08:00–19:30	23.5 × 15.7 mm CCD	3040 × 2024	DSLR camera	~N; 0°	Bater et al. (2011)
Harvard Forest[b]	Canon; A560	h; 07:00–20:00	1/2.5″-type CCD	3072 × 2304	P-and-S camera	~N; ~20°	This study
Howland Forest	StarDot; NetCam XL 1MP	hh; 04:00–21:30	1/2″-type CMOS	1024 × 768	Out. webcam	~N; ~20°	Richardson et al. (2009a)
Morgan Monroe State Forest	StarDot; NetCam SC 1.3MP	hh; 04:00–21:30	1/2.5″-type CMOS	1296 × 976	Out. webcam	~N; ~20°	Richardson et al. (2009a)
Niwot Ridge	Canon; VB-C10R	2-h; 06:00–20:00	1/4″-type CCD	640 × 480	In. webcam	~N; ~20°	This study
Pasayten Wilderness	Olympus; C-730	3-h; 09:00–15:00	1/2.7″-type CCD	1600 × 1200	DSLR camera	~SW; 0°	This study
Smoky Purchase-Knob	Olympus; E-420	h; 07:00–19:00	Live MOS (n.s.f.)	640 × 480	DSLR camera	~NE; 0°	This study
Shining Rock Wilderness	Olympus; SP-500	3-h; 09:00–15:00	1/2.5″-type CCD	1536 × 1024	DSLR camera	~NW; 0°	This study

[a] This digital camera is approximately similar to the Olympus DSLR cameras used by the USDA Forest Service Air Resource Management program and National Park Service Air Resources program.
[b] Digital cameras for the intercomparison were mounted on an ancillary instrumentation tower at Harvard Forest located approximately 130 m southwest of the EMS instrumentation tower.
[c] The manufacturer declined to release information on the imaging sensors.

At Niwot Ridge, images were taken at 2-hour-intervals with an indoor webcam, transferred via FTP (push), and also stored on the PhenoCam server. All of the above indoor/outdoor webcams were contained in inexpensive outdoor camera housings (e.g., VT-EH10; Vitek Industrial Video Products, Valencia, CA, USA) mounted on instrumentation towers, overlooking the landscape and thus the top of the forest canopy at shallow tilt angles from the horizontal (Table 2).

The USDA Forest Service and National Park Service installed Olympus DSLR cameras (Dolly Sods Wilderness; Pasayten Wilderness; Shining Rock Wilderness; Smoky Purchase Knob; Grand Canyon) for visibility and air quality monitoring at look-outs and vantage points with tilt angles of ∼0° (=horizontal view). At these sites, images were taken at lower frequencies, ranging from hourly to three-hourly intervals (Table 2). The Olympus DSLR cameras at these sites were controlled with proprietary software for digital camera configuration, image capture and Internet transfer (Dee Morse [Environmental Protection Specialist, Air Resources Division], *personal communication*; Emily Vanden Hoek [Network Operations Manager, Air Resource Specialists, Inc.], *personal communication*). For their integration in the PhenoCam network, images from these digital cameras were retrieved via HTTP (pull) and stored on the PhenoCam server.

3.2.2. Digital camera and image file format choice

To assess the role of digital camera choice for *ExG* and g_{cc}, we installed eleven digital cameras including web-, plant- and game-cams, and digital P-and-S and DSLR cameras at Harvard Forest from August through November 2010 (Table 2). This period is characterized by substantial changes in canopy greenness during leaf senescence and abscission (Richardson et al., 2009a). With the chosen digital cameras we attempted to cover a wide spectrum of digital camera types currently in use at AmeriFlux sites (Richardson et al., 2007, 2009a) or reported from other sites and studies (Ahrends et al., 2009; Bater et al., 2011; Kurc and Benton, 2010; Sonnentag et al., 2011).

All digital cameras were attached next to one another on a wooden plank mounted at a height of 24 m on an ancillary instrumentation tower, located approximately 130 m southwest of the Harvard Forest EMS instrumentation tower (Table 2). Eight of the digital cameras were contained in outdoor camera housings (VT-EH10; Vitek Industrial Video Products), whereas three were designed as self-contained units for outdoor applications with no external power and Internet access (PlantCam WSCA04; Moultrie Game Spy I-60; Pentax K100D).

Images from the six outdoor webcams were taken at half-hourly intervals and transmitted to the PhenoCam server via FTP. The two indoor webcams lack internal FTP servers. Images from these two cameras were taken at the same interval, and retrieved by first pulling an image via HTTP to a personal computer at the site, and then by transmitting it via FTP for integration in the PhenoCam network.

Images from the PlantCam WSCA04, the Moultrie Game Spy I-60, the Canon A560 and the Pentax K100D were also taken at half-hourly or hourly intervals, stored on 4GB flash memory cards, and retrieved during weekly to bi-weekly visits to Harvard Forest. The PlantCam WSCA04 and the Moultrie Game Spy I-60 were primarily designed for repeat photography (PlantCam WSCA04) or repeat and motion detection-triggered photography (Moultrie Game Spy I-60). Repeat photography with the Pentax K100D was implemented with the Digisnap 2100 electronic shutter release/intervalometer as part of Harbortronic's Time-Lapse Package (Harbortronics, Fort Collins, CO, USA). To perform repeat photography with the Canon A560, we wrote an intervalometer script in uBASIC, the scripting language for the Canon Hack Development Kit (CHDK; http://chdk.wikia.com/).

Images from all digital cameras of Table 2 recorded *RGB* brightness levels and were stored as uncompressed 24-bit JPEG files, except for images taken with the Pentax K100D, which were stored as RAW files. These were converted to uncompressed 24-bit JPEG files using the Unidentified Flying RAW (UFRAW) utility (http://ufraw.sourceforge.net/). In addition, we used the Pentax K100D image archive to examine whether the information lost in the conversion from RAW to JPEG actually matters for phenological research.

The above digital cameras were overlooking the forest canopy top at shallow tilt angles of ∼20° or at ∼0° (Table 2). Consequently, their field-of-views (FOV) contained different amounts of sky resulting in differences in overall scene brightness between cameras due to the high variability in sky brightness. In addition, the presence of clouds may have introduced additional shading, thus making parts of the forest canopy appear darker. Together, these effects most likely affected the cameras' metering system to determine exposure settings (i.e., aperture and shutter speed).

The digital cameras of Table 2 differ widely in terms of configuration options, ranging from no options at all (e.g., PlantCam WSCA04; Moultrie Game Spy I-60) to numerous options to fully control (e.g., Canon A560; Pentax K100D) photographic properties, resolution and light sensitivity. We kept most configuration settings on default, but, when possible, we set *Exposure* to "Automatic", and *White Balance* to "Manual" (e.g., Canon A560) or "Keep current value" (e.g., Vivotek IP6122) or, correspondingly, *Color Balance* to "Manual" (e.g., StartDot NetCam XL 3MP) following Richardson et al. (2009a).

Most image archives used in this study were characterized by gaps of various lengths (<day to several weeks) due to different technical issues including power outage, loss of Internet connection, and battery leakage or failure.

3.3. Ancillary data sets

We used two ancillary data sets to aid in the interpretation of *ExG* and g_{cc} obtained from the different cameras at Harvard Forest and Howland Forest: observer-based estimates of spring and autumn phenology to better characterize the seasonality of *ExG* and g_{cc} in terms of actual phenological changes, and incoming photosynthetically active radiation to characterize overall atmospheric transmittance conditions (Harvard Forest only).

At Harvard Forest, spring and autumn phenology of several hardwood tree species have been observed since 1990 at three-to-seven day intervals (Richardson et al., 2006; Richardson and O'Keefe, 2009). In our study we used field observations from four red oak trees (2009 and 2010) in close proximity to the Harvard Forest EMS and ancillary instrumentation towers. Similar field observations were made on several red spruce, eastern hemlock, and red maple trees at Howland Forest at the same intervals, also since 1990 (Richardson et al., 2009b).

Incoming photosynthetically active radiation (*PAR*) at Harvard Forest was measured as photosynthetic photon flux density (μmol m^{-2} s^{-1}) with a quantum sensor (LI-190; Licor, Lincoln, NE, USA) at a height of 24 m on the ancillary instrumentation tower. The measurements were logged by a data logger (CR10; Campbell Scientific, Logan, UT, USA) at 5 s intervals and recorded as half-hourly mean values.

3.4. Analyses

3.4.1. Scene illumination changes

To examine the influence of seasonal, weather-related and diurnal variations in scene illumination and thus resulting *RGB* brightness levels, our initial focus was on two contrasting sites

Harvard Forest

a) overcast   b) sunny

Howland Forest
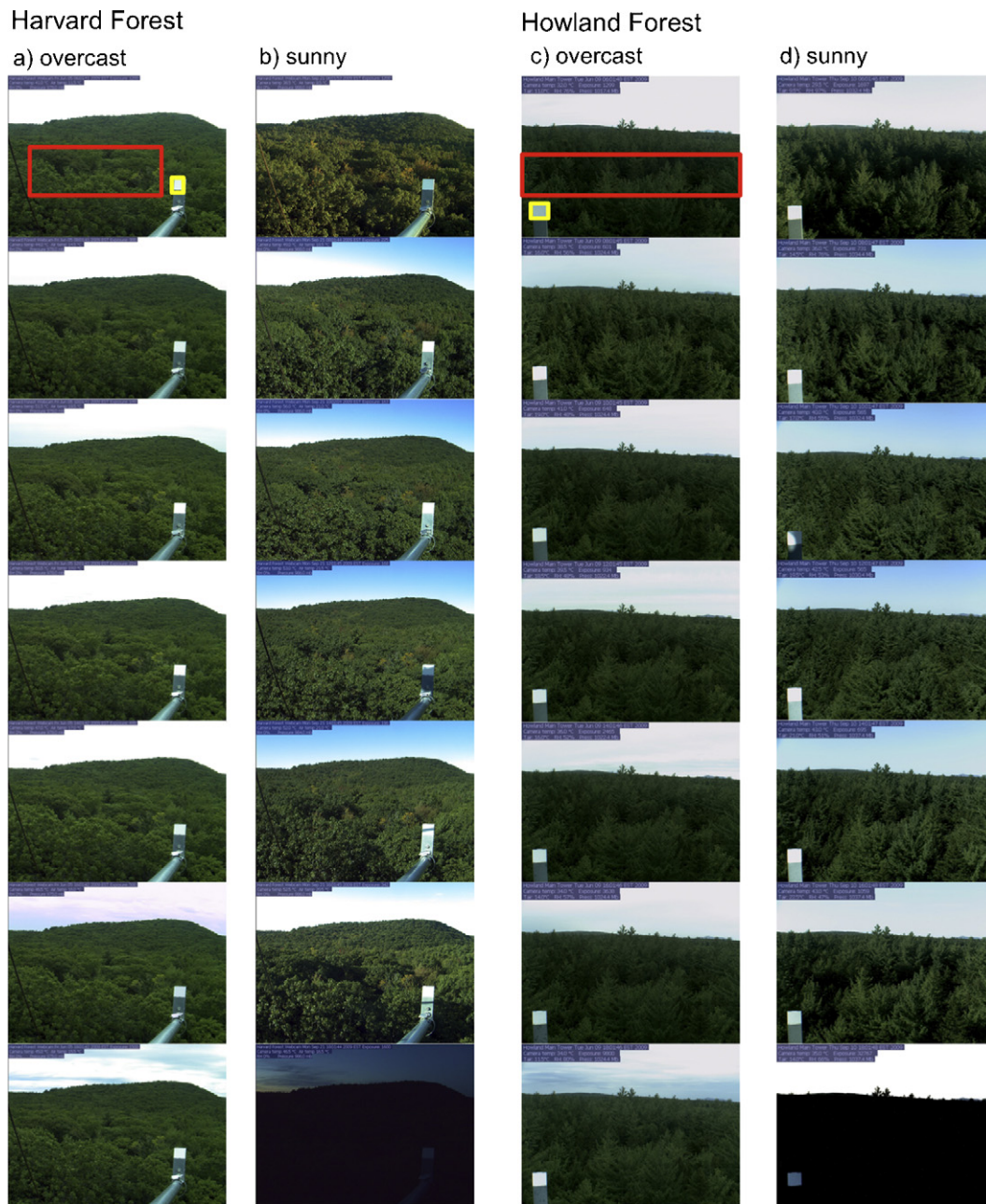
c) overcast   d) sunny

Fig. 1. Example images (from top to bottom: 06:00; 08:00; 10:00; 12:00; 14:00; 16:00; 18:00 h local time) from deciduous-dominated Harvard Forest during (a) an overcast (DOY 156) and (b) a sunny day (DOY 264), and from coniferous-dominated Howland Forest during (c) an overcast (DOY 160) and (d) a sunny (DOY 253) day from summer 2009. The red and yellow rectangles are the regions-of-interests for the dominant tree species and the reference panels, respectively. (For interpretation of the references to color in this figure legend, the reader is referred to the web version of the article.)

using all available images from 2009: the deciduous-dominated Harvard Forest and the coniferous-dominated Howland Forest (also used by Richardson et al., 2009a).

We selected regions-of-interest (ROI) representative of the dominant tree species at both Harvard Forest and Howland Forest (Fig. 1; Table 1). For each available digital image, we extracted ROI-averaged RGB brightness levels for which we calculated ExG (Eq. (1)) and g_{cc} (Eq. (2)).

To examine the effects of seasonal changes in scene illumination on ExG and g_{cc} and as a quality check regarding the stability of the obtained vegetation signal, we selected a second ROI covering the light-grey reference panels for which we also extracted ROI-averaged RGB brightness levels to calculate reference ExG (ExG_{ref}) and g_{cc} (g_{cc_ref}). At both sites the reference panels were installed in

a way to minimize the likelihood of shading by the tower or the camera housing during mid-day hours.

For each of the two sites, we classified one digital image from around noon (local time) according to five weather conditions into "Snow", "Fog; water on camera housing window; etc.", "Overcast", "Partially overcast" and "Sunny" through visual inspection by the same person to examine the influence of weather conditions on ExG and g_{cc}.

Next, to assess the effects of diurnal changes in illumination intensity on ExG and g_{cc}, we categorized all available winter (day-of-year [DOY] 1–50 and 330–365) and summer (DOY 150–280) images in 2009 into "sunny" and "overcast" through visual inspection (again, by the same person) for both sites. The two periods of the year were defined to approximately obtain stationary time

series of *RGB* brightness levels. We defined a sunny day in each period when all available images had less than approximately 10% cloud cover and the forest canopy was illuminated by direct sunlight. Similarly, we defined an overcast day when all images had more than approximately 90% cloud cover and, consequently, did not receive any direct sunlight. Not surprisingly, during sunny days the forest canopy at Harvard Forest and Howland Forest appeared brighter than during overcast days (Fig. 1). We identified significant differences in the mean diurnal patterns of *ExG* and g_{cc} for sunny and overcast days for both winter and summer periods using the Wilcoxon signed-rank test with $\alpha = 0.05$.

3.4.2. Statistical methodology

Our initial hypothesis was that significant differences in mean diurnal *ExG* and g_{cc} between overcast and sunny days would be reflected as unwanted reductions in daily *ExG* and g_{cc} when simply calculated from *mean* mid-day or mid-morning ROI-averaged *RGB* brightness levels or from ROI-averaged *RGB* brightness levels of one representative image (e.g., Ahrends et al., 2008, 2009; Richardson et al., 2009a; Sonnentag et al., 2011).

For comparison with *ExG* and g_{cc} based on *mean* mid-day (*mmd*) values between 10:00 and 14:00 h local time, we propose the following moving-window approach based on all available daytime images. These were selected by filtering for night-time or "dark" images from around sunrise or sunset by simple *RGB* thresholding, i.e., ROI-averaged *RGB* triplets with brightness levels below a predefined *DN* threshold were discarded. Visual selection of these thresholds was unambiguous given the disjoint day-time vs. nighttime distributions of *RGB* brightness levels (data not shown). Within a three-day window (step-size: three days) we assigned the 90th percentile of all daytime values of *ExG* and g_{cc} to the window center day (*per90*). Thus, this approach resulted in three-day time series of *ExG* and g_{cc}.

We assessed the performance of the two approaches, *mmd* and *per90*, for Harvard Forest and Howland Forest and ten additional sites (Table 1). First, we discarded *ExG* and g_{cc} from night-time and "dark" images camera-specific *RGB* thresholding. Next, we fitted non-parametric smoothed curves to three-day *ExG* and g_{cc} obtained from *per90* and corresponding daily values from *mmd* using local polynomial regression fitting (Loess curve; Cleveland, 1979; Cleveland and Devlin, 1988) with a low degree of smoothing (span = 0.30). The main criterion for performance comparison was the root mean square error (RMSE) calculated from the difference between observed and fitted *ExG* and g_{cc}. With the chosen three-day window and step size, the errors between observed and fitted *ExG* and g_{cc} were approximately normally distributed.

3.4.3. Digital camera choice

For the digital camera intercomparison at Harvard Forest (Table 2), we followed a similar procedure as outlined in Section 3.4.2: first, we discarded *ExG* and g_{cc} from night-time and "dark" images based on camera-specific *RGB* thresholding prior to calculating three-day and corresponding daily values of *ExG* and g_{cc} with *per90* and *mmd*, respectively, and the final fitting of Loess curves. Next, we determined the DOYs corresponding to the 20th, 30th, 40th, 50th, 60th, 70th, and 80th percentiles of each Loess curve (spanning from DOY 270 to the DOY corresponding to each Loess curve's minimum value) to examine their agreement at different stages of senescence.

3.4.4. Image file format choice

To examine whether the information lost in the conversion from unprocessed RAW to compressed, "lossy" JPEG affects *ExG* and g_{cc}, we examined their diurnal patterns calculated for two periods (DOY 254–259 and DOY 300–314) in autumn 2010 from images with

increasing compression rates, ranging from uncompressed [0%], 50%, 75% and 97% compression.

All analyses (3.4.1–3.4.4) were done in the R computing environment (v2.10.0; R Development Core Team, 2009) and the scripts developed for this study are available from the authors on request.

4. Results

4.1. Scene illumination changes

We examined the stability of the vegetation signals obtained at Harvard Forest and Howland Forest based on ROI-averaged *RGB* brightness levels and their standard deviations per image. The visual inspection of *RGB DN* time series obtained from all available images did not indicate that *ExG* and g_{cc} were affected by imaging sensor degradation or other technical issues. In contrast to ExG_{ref}, g_{cc_ref} show negligible seasonal patterns, suggesting that g_{cc_ref} was more effective than ExG_{ref} in suppressing seasonal effects of changes in scene illumination with summer months generally being brighter than winter months (Fig. 2a–d).

The standard deviations of *RGB DN* vary at both sites for 2009 (Fig. 2e and f). The brightness levels of the three color channels are basically identical (i.e., $R{:}G{:}B \approx 255{:}255{:}255$) when the reference panel was well-lit under sunny conditions, causing the pixels of the reference ROI to saturate (i.e., low standard deviation in Fig. 2e and f), thus limiting the usefulness of the panel to serve as a reference. However, the reference brightness levels differ under most other atmospheric transmittance conditions as these cause a wide range of different scene illuminations over a day (e.g., mid-day vs. non-mid-day hours) and the year. Under these different scene illuminations, the reference panel was seen by the digital cameras in various shades of grey contaminated by other color hues (i.e., high standard deviation in Fig. 2e and f).

The lack of seasonal patterns in *ExG* and g_{cc} at Grand Canyon compared to Harvard Forest and Howland Forest highlights the influence of vegetation phenology (and not just changes in incoming solar radiation and thus scene illumination) on the color signal captured by digital cameras (Fig. 3a and b). At deciduous-dominated Harvard Forest, both *ExG* and g_{cc} started to increase in spring in response to bud break after an essentially stable, dormant winter period (Fig. 3c and d). Compared to observer-based estimates of spring and autumn phenology, the two descriptors of canopy greenness peaked when around 50% of all leaves had reached 75% of their final length, and in the following remained stable throughout the summer when the forest canopy was fully developed. Both *ExG* and g_{cc} started to decrease with continued canopy coloring during senescence, and reached their lowest values when all leaves had changed their colors. After a following sharp increase with continued leaf abscission, *ExG* and g_{cc} returned to their stable winter levels (dormancy). In contrast, the seasonality of *ExG* and g_{cc} was weaker at coniferous-dominated Howland Forest (Fig. 3e and f).

Changes in scene illumination due to changes in weather conditions affected *ExG* at Harvard Forest throughout the year, but their influences were largely suppressed in g_{cc} (Fig. 3c and d). Especially *ExG* was generally decreased under overcast compared to sunny conditions, but such a reduction was not present in g_{cc}. In contrast, *ExG* was again reduced under overcast compared to sunny conditions at Howland Forest, but the suppression of weather-related changes in scene illumination with g_{cc} was less effective; g_{cc} was almost as variable as *ExG* (Fig. 3e and f).

As to be expected from Fig. 3, mean diurnal patterns in *ExG* for sunny and overcast days were significantly different in summer at both Harvard Forest and Howland Forest, especially during
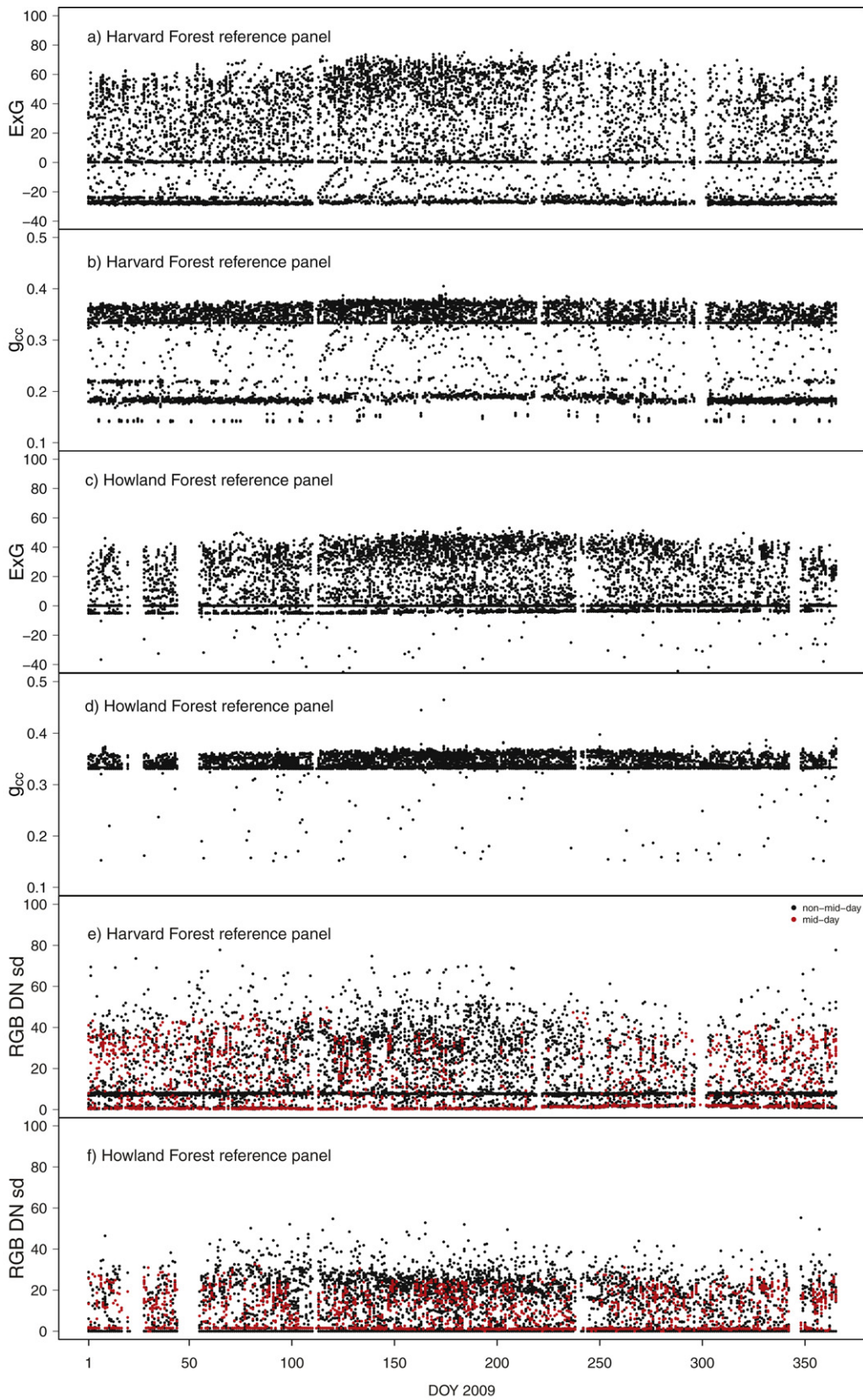
Fig. 2. Reference panel (a) *excess green* (*ExG*), and (b) green chromatic coordinate (*g_{cc}*) for Harvard Forest, reference panel (c) *ExG*, and (d) *g_{cc}* for Howland Forest, (e) *RGB* standard deviation (sd) for Harvard Forest (yellow rectangle region-of-interest [ROI] in Fig. 1a), and (f) *RGB sd* for Howland Forest (yellow rectangle ROI in Fig. 1b). Mid-day covers the period between 10:00 and 14:00 h (local time), whereas non-mid-day hours covers periods before 10:00 and after 14:00 h. (For interpretation of the references to color in this figure legend, the reader is referred to the web version of the article.)

Table 3

Comparison of root mean square errors between observed and fitted three-day *excess green* (*ExG*) and the green chromatic coordinate (*g_{cc}*) obtained as *mean* mid-day values (*mmd*) and as the 90th percentile of all day-time values (*n_{filter}*) within a three-day moving window (*per90*) for twelve sites (Table 1). Day-time values were selected by filtering for night-time or "dark" digital images by *RGB*-thresholding (digital number (*DN*) threshold). Also given are results obtained when using "optimum" percentile (*perOpt*) instead of the 90th percentile (see text for more explanation).

Site	n_{total}	DN threshold	n_{filter}	ExG			g_{cc}		
				mmd	*perOpt*[a]; *per90*[a]	% change (*perOpt*; *per90*)	*mmd* ($\times10^3$)	*perOpt*[a] ($\times10^3$); *per90*[a] ($\times10^3$)	% change (*perOpt*; *per90*)
Arbututs Lake	13,155	20	8846	4.14	2.19 (50); 3.32 (90)	−47; −20	6.27	4.59 (90); 4.59 (90)	−27; −27
Bartlett Forest	2895	40	2479	2.99	2.14 (80); 2.25 (90)	−28; −25	2.61	2.16 (60); 2.44 (90)	−17; −7
Chibougamau	11,613	35	7284	2.64	1.82 (80); 1.90 (90)	−31; −28	3.37	2.27 (80); 2.33 (90)	−33; −31
Dolly Sods Wilderness	4231	20	3805	7.11	3.39 (90); 3.39 (90)	−52; −52	11.15	5.71 (60); 5.86 (90);	−53; −52
Grand Canyon	3991	60	3125	2.47	1.12 (60); 1.91 (90)	−55; −23	2.29	1.10 (70); 1.71 (90)	−52; −26
Harvard Forest	12,171	35	8000	3.91	3.07 (50); 3.21 (90)	−21; −18	5.38	4.45 (50); 4.45 (90)	−17; −17
Howland Forest	11,846	10	8079	2.43	1.41 (60); 1.48 (90)	−42; −39	12.51	6.95 (90); 6.95 (90)	−44; −44
Morgan Monroe State Forest	10,338	45	6186	3.27	2.01 (90); 2.01 (90)	−38; −38	5.13	3.08 (80); 3.08 (90)	−40; −40
Niwot Ridge	2748	80	2117	7.96	5.21 (80); 5.22 (90)	−34; −34	6.64	4.33 (90); 4.34 (90)	−35; −35
Pasayten Wilderness	4745	5	4252	4.53	2.26 (50); 2.62 (90)	−50; −42	7.11	3.22 (80); 3.47 (90)	−55; −51
Smoky Purchase-Knob	4159	10	3831	5.17	3.29 (50); 3.90 (90)	−36; −25	8.51	4.16 (90); 4.16 (90)	−51; −51
Shining Rock Wilderness	957	–	957	8.48	3.71 (50); 4.30 (90)	−56; −49	8.25	5.37 (50); 7.17 (90)	−35; −13

[a] Number in brackets denotes the percentile.

mid-day hours when the Sun was highest (Fig. 4a and b). The differences between overcast and sunny days were reduced but still significant for g_{cc} at both sites (Fig. 4c and d). Similar mean diurnal patterns for *ExG* and g_{cc} and especially significant differences between overcast and sunny days were present in winter at both Harvard Forest and Howland Forest (data not shown).

Based on Figs. 3 and 4 it is evident that calculating daily values of g_{cc} and especially *ExG* based on *mmd* might introduce substantial unwanted variability due to diurnal and weather-related variations in scene illumination, i.e., variability not related to phenological changes in canopy greenness. By using g_{cc} instead of *ExG* these influences were reduced but not fully removed.

4.2. Statistical methodology

As an attempt to further reduce the influence of diurnal and weather-related variations in scene illumination on *ExG* and g_{cc}, we propose *per90*, a moving-window approach that assigns the 90th percentile of *ExG* and g_{cc} to the center day (i.e., resulting in one daily value every third day), as opposed to daily values of *ExG* and g_{cc} obtained with *mmd* (i.e., from *mean* mid-day *ExG* and g_{cc}). We compared the performance of *per90* and *mmd* based on RMSE calculated from the difference between three-day *ExG* and g_{cc}, and the fitted Loess (Table 3): *per90* reduced RMSE for both *ExG* and g_{cc} on average by 34% compared to *mmd*. To check if the 50th, 60th, 70th, 80th or 90th percentile would be more appropriate, we also examined the "optimum" percentile (chosen as the percentile producing the lowest RMSE), *perOpt*, which on average reduced RMSE between *mmd* and *perOpt* by 41% (*ExG*) and 39% (g_{cc}).

Examples for daily *ExG* and g_{cc} at deciduous-dominated (Harvard Forest; Morgan Monroe State Forest) and coniferous-dominated (Howland Forest; Chibougamau) forest sites are shown in Figs. 5 and 6, respectively. In addition to the quantitative comparison of Table 3, it is evident from the visual inspection that *per90* was successful in reducing unwanted variability related to changes in illumination intensity for both *ExG* and g_{cc} compared to the respective values obtained with *mmd*.

4.3. Digital camera choice

As described in Section 3.4.3, we compared a broad range of digital cameras with different imaging sensors (CMOS vs. CCD vs. Live MOS) and thus different photographic properties, resolutions,

and light sensitivities as reflected in quality (e.g., contrast, sharpness, noise) and visual appearance of the obtained digital images. Their most striking features are the inherent differences among digital cameras in default color balances (Fig. 7a–h). For example, images taken with the StarDot NetCam SC 1.3MP (Fig. 7e) and the Vivotek IP7160 (Fig. 7g) were generally dominated by colder tones ('greenish' and 'bluish', respectively), whereas the Axis 211 (Fig. 7c) produced images that were dominated by warmer tones ('reddish').

The different digital cameras were overlooking the same portion of the forest canopy top at Harvard Forest, here mostly dominated by red oaks (red ROI in Fig. 7). Red oak leaves are characterized by dark-red fall colors, which cause a seasonal pattern in r_{cc} opposite to g_{cc} (Fig. 8a). After a steady increase over the summer, r_{cc} starts to rapidly increase in autumn at around DOY 275, reaching maximum values corresponding to minimum values of g_{cc} when all leaves are colored just prior abscission (i.e., "100% leaves colored/20–33% leaves abscissed" in Fig. 8a). With ongoing leaf abscission, r_{cc} decreases rapidly, causing increases in both g_{cc} and b_{cc} (data not shown) as the sum of the rgb chromatic coordinates equals to one (i.e., the canopy becomes less red but relatively more green and blue).

Due to differences in overall image color balance, time series of three-day *ExG* (*per90*) and g_{cc} from different digital cameras were shifted over a wide range (Fig. 8b–e). Consequently, their absolute values were not directly comparable. However, the overall temporal patterns were roughly similar despite differences in the magnitude of their seasonal amplitudes. All time series show a decrease over time, thus reflecting continued canopy color changes from green over dark-red/reddish-brown to brown. Minimum (maximum) values in *ExG* and g_{cc} (r_{cc}; data not shown) were reached when all leaves had changed their colors. Over the following two weeks, both *ExG* and g_{cc} increased again with continued leaf abscission toward their winter levels characteristic for dormancy.

Unfortunately, battery leakage in the Moultrie Game Spy I-60 and battery failure in the Pentax K100D resulted in large gaps (several weeks) for those cameras. However, most time series of *ExG* and g_{cc} and their best-fit Loess curves show only little or no multi-day divergence among the different digital cameras, except for the three Axis models and especially the D-Link DCS-920 (Fig. 8b–e). Visual inspection in addition to inspection of mean daily *PAR* revealed that the combination of specific weather-related changes in illumination intensity together with canopy color changes were responsible for the week-to-week variations for some cameras (Fig. 8b and c).
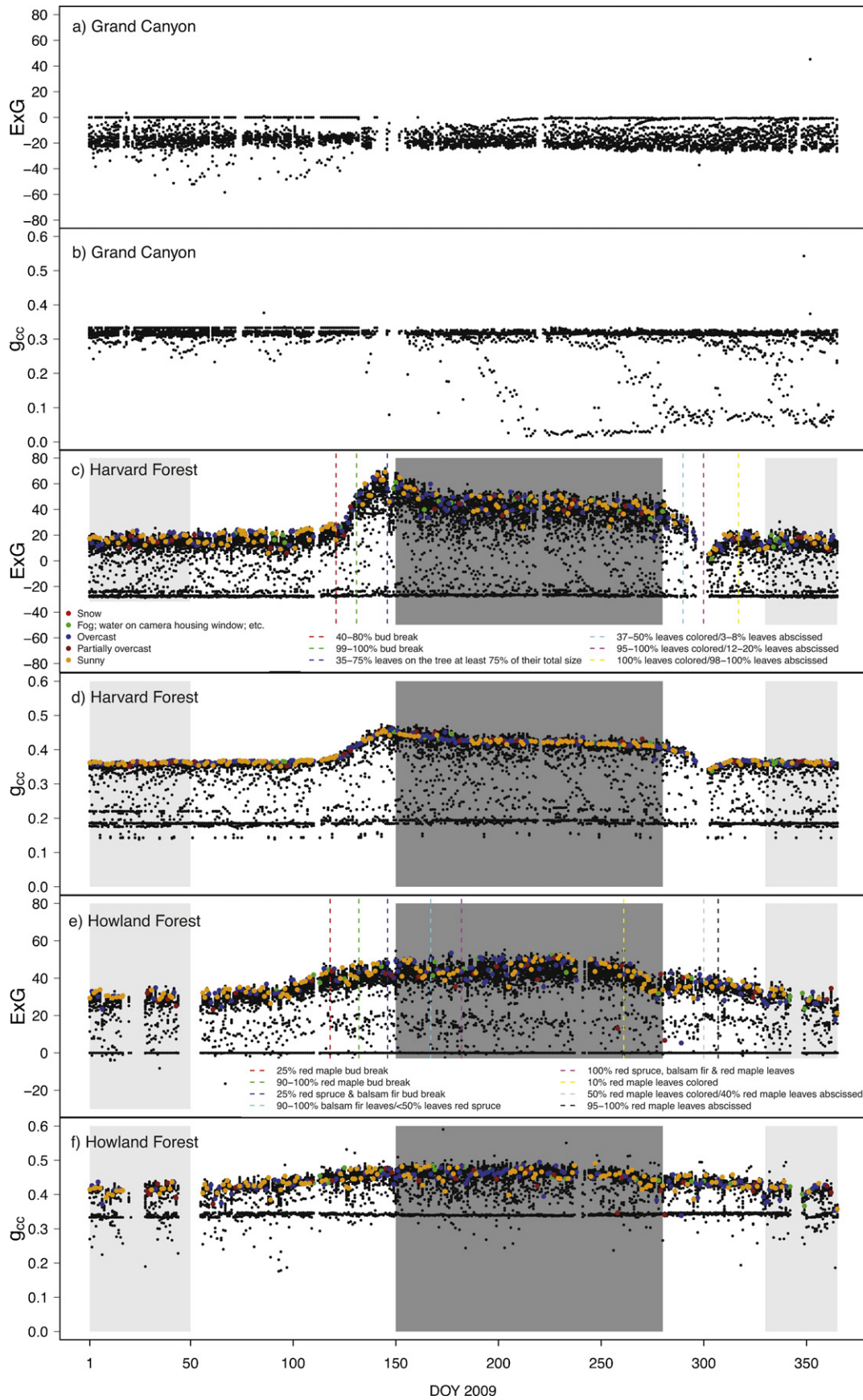
Fig. 3. Example data set of (a) *excess green* (*ExG*) and (b) the green chromatic coordinate (*g$_{cc}$*) for Grand Canyon, of (c) *ExG* (including observer-based estimates of spring and autumn phenology for red oak [O'Keefe, 2000]) and (d) *g$_{cc}$* for Harvard Forest, of (e) *ExG* (including observer-based estimates of spring and autumn phenology for red spruce, eastern hemlock, and red maple [Richardson et al., 2007]) and (f) *g$_{cc}$* for Howland Forest (red rectangle region-of-interests for the dominant tree species in Fig. 1a and b). The
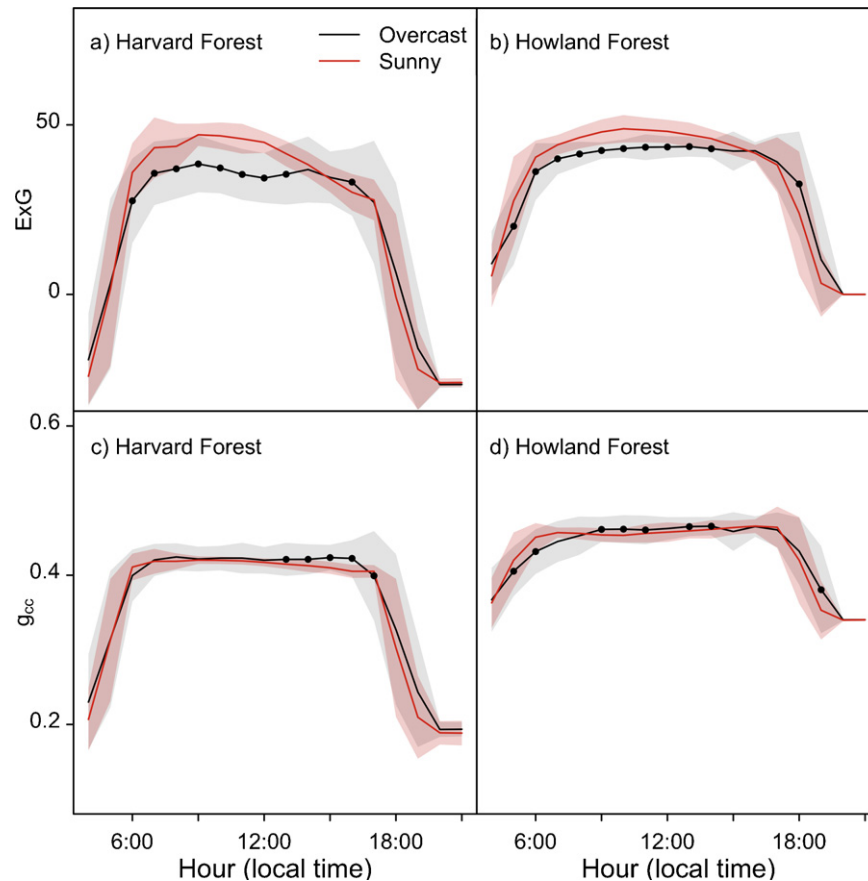
Fig. 4. Mean diurnal patterns (±one standard deviation [shaded areas]) of *excess green* (*ExG*) at (a) Harvard Forest and at (b) Howland Forest, and of the green chromatic coordinate (*g_cc*) at (c) Harvard Forest and at (d) Howland Forest for overcast and sunny days (see text for further explanation) over the summer period in 2009 (dark-grey shading in Fig. 2). The black dots indicate significant differences between the overcast and sunny conditions (Wilcoxon signed-rank test; $p < 0.05$). (For interpretation of the references to color in this figure legend, the reader is referred to the web version of the article.)

For example, the drop in *ExG* and g_{cc} for the D-Link C920 between DOY 278 and DOY 288 occurred in a period of sunny autumn days following and preceding several overcast days. As a consequence of starting autumn color changes in red oak leaves, red and blue brightness levels increased substantially almost reaching saturation compared to decreasing green brightness levels, overall causing a substantial drop in *ExG* and g_{cc} (data not shown).

To quantify the agreement in *ExG* and g_{cc} for different digital cameras over the observation period, we compared DOY corresponding to a range of percentiles (20th–80th) for Loess curves fitted to three-day *ExG* and g_{cc} (*per90*; Fig. 9). In addition, we compared DOY of the minimum values of the fitted Loess curves, corresponding to complete coloring of all leaves (i.e., "100% leaves colored/20–33% leaves abscissed"; Fig. 8a). Generally, there was a wider spread between the different cameras at the higher percentiles (50th–90th) than at the lower percentiles (10th–40th), especially for g_{cc} (Fig. 9b). This indicates that the cameras responded differently to canopy color changes, especially during earlier stages of senescence, but were in overall agreement toward the end. There was slightly better agreement between cameras for *ExG* (DOY standard deviations [$n = 9$]: 1.2, 1.6, 1.6, 4.9, 5.8, 2.7, 3.1, 3.5 and 5.5 for the 10th–90th percentiles) than for g_{cc} (DOY standard deviations [$n = 9$]: 1.3, 1.6, 1.7, 5.0, 2.4, 6.0, 5.6, 5.3 and 4.7 for the 10th–90th percentiles). After excluding *ExG* and g_{cc} from the D-Link DCS-920 (Fig. 8c) due to their substantial week-to-week

variations (e.g., both *ExG* and g_{cc} were outside the 1.5 times the interquartile range at different percentiles), the DOY standard deviations ($n = 8$) between *ExG* (1.3, 1.7, 1.6, 2.0, 2.4, 2.8, 3.1, 3.3 and 4.6 for the 10th–90th percentiles) and g_{cc} (1.4, 1.7, 1.8, 2.2, 2.5, 3.3, 3.3, 3.7 and 4.3 for the 10th–90th percentiles) were basically identical (data not shown). At complete leaf coloring, the DOY standard deviation ($n = 8$) was 1.3 for *ExG* but dropped further to 1.1 for g_{cc}.

4.4. Image file format choice

Due to battery failure and other technical issues, the image archive for the Pentax K100D covers only two short periods when the canopy was still fully developed in late summer (∼DOY 255) and after essentially all leaves had changed their colors in late autumn (∼DOY 310). To examine the role of information loss due to RAW-to-JPEG conversion for phenological research based on canopy greenness, we calculated late-summer and fall g_{cc} with increasing compression rates (Fig. 10a–j). Increased compression rates resulted in increased posterization of images (reduction in displayed color tones) and associated abrupt changes between different colors and tones (e.g., sky color tones in Fig. 10a and b). However, up to unrealistic compression rates (here: 97%), the mean diurnal patterns of g_{cc} in late summer and autumn remained essentially constant (Fig. 10i and j).

---

color encoding in panels (c)–(f) indicates daily weather conditions in the images at around noon (local time) as classified by visual inspection (color key is provided in panel (c)). The light- and dark-grey shading in panels (c)–(f) indicates winter and summer periods in 2009 (see text for further explanation). (For interpretation of the references to color in this figure legend, the reader is referred to the web version of the article.)
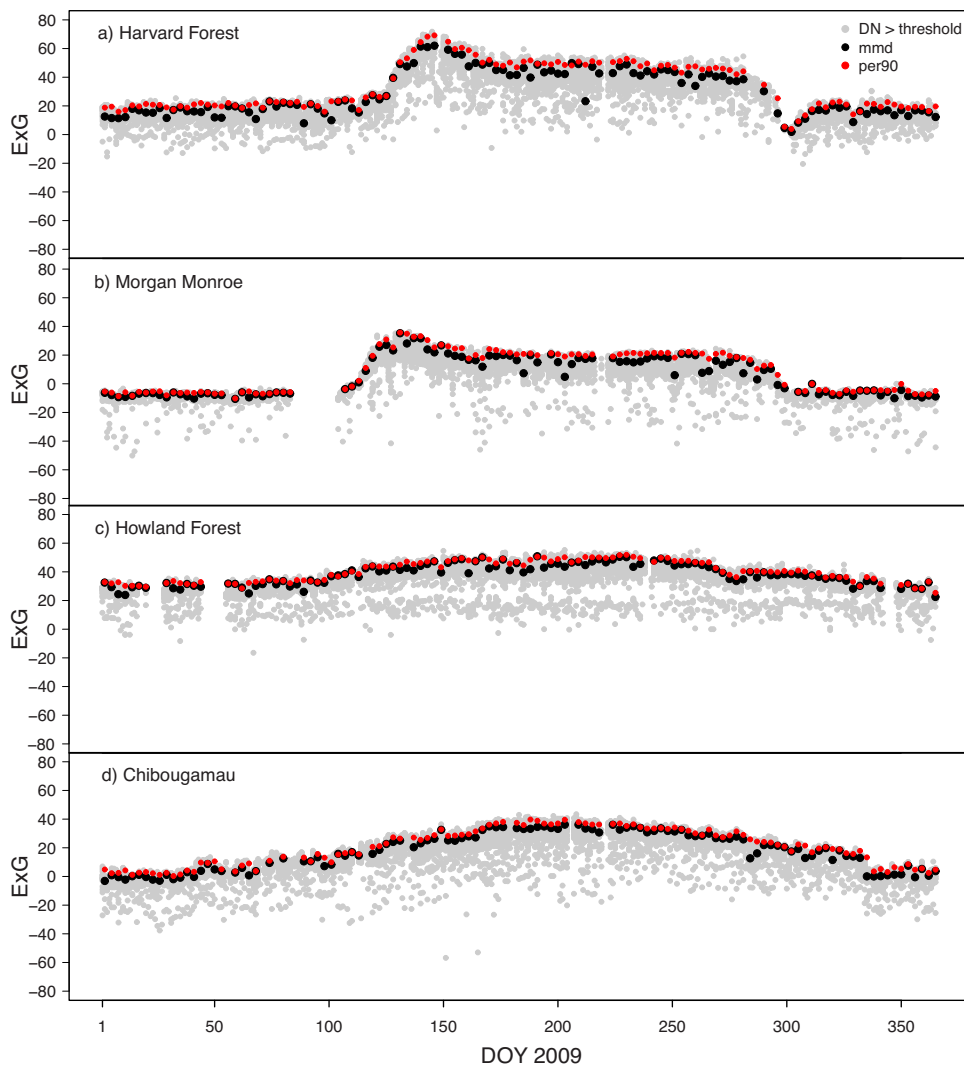
Fig. 5. Three-day *green excess* (*ExG*) obtained as mean mid-day values (*mmd*) and as the 90th percentile of all day-time values within a three-day moving window (*per90*) at two deciduous-dominated forest sites: (a) Harvard Forest and (b) Morgan Monroe State Forest, and at two coniferous-dominated forest sites: (c) Howland Forest and (d) Chibougamou (Table 1). The green chromatic coordinate was filtered for digital camera-specific *RGB* thresholds (digital number (*DN*) > threshold; see Table 3 and text for further explanation). (For interpretation of the references to color in this figure legend, the reader is referred to the web version of the article.)

5. Discussion

A series of recent studies has demonstrated the potential use of high-frequency repeat photography with conventional digital cameras to continuously monitor vegetation canopies for phenological research (Ahrends et al., 2008, 2009; Ide and Oguma, 2010; Kurc and Benton, 2010; Richardson et al., 2007, 2009a; Sonnentag et al., 2011). The idea behind the use of consumer-grade digital cameras for that purpose is simple: separate extraction of *RGB* brightness levels allows for the calculation of color indices that describe changes in canopy color over time.

Overall, we observed two distinct seasonal patterns in canopy color characteristic for coniferous- and deciduous-dominated forests. As suggested previously, the seasonality of canopy greenness at coniferous-dominated forest sites such as Howland Forest seems to be largely controlled by changes in leaf pigmentation (e.g., Ensminger et al., 2004) of existing foliage, rather than development and senescence of new needle foliage (Richardson et al., 2009a). Open questions remain, however, as to whether some aspects of the seasonal trajectory of canopy greenness, particularly the well-defined "spring peak" in canopy greenness observed at Harvard Forest and other deciduous-dominated forest sites is related to

changes in leaf physiology and pigmentation, changes in canopy structure (i.e., leaf size, shape, orientation) or some combination thereof. We are currently addressing these questions in a follow-up study at Harvard Forest (April–November, 2011).

It is important to acknowledge that consumer-grade digital cameras are not calibrated scientific instruments. Several important questions start to emerge especially when using image archives obtained from different cameras with different, often unknown, settings, different illumination and viewing geometries, and different image file formats from different sites. With this study we attempt to answer questions related to changes in scene illumination and their link to widely used descriptors of canopy greenness, *ExG* and *g*$_{cc}$ (Section 5.1), and digital camera and image file format choice (Section 5.2).

In another follow-up study at Harvard Forest (July–November 2011) we are comparing the vegetation signals obtained from a NIR-enabled webcam with various tower-based spectral measurements made with photodiodes (Garrity et al., 2010), light-emitting diodes (Ryu et al., 2010), a spectroradiometer (http://www.ppsystems.com/unispec_dc.htm) and commercially-available broadband (http://www.kippzonen.com/) and narrow-band (http://www.skyeinstruments.com/) radiometric sensors.
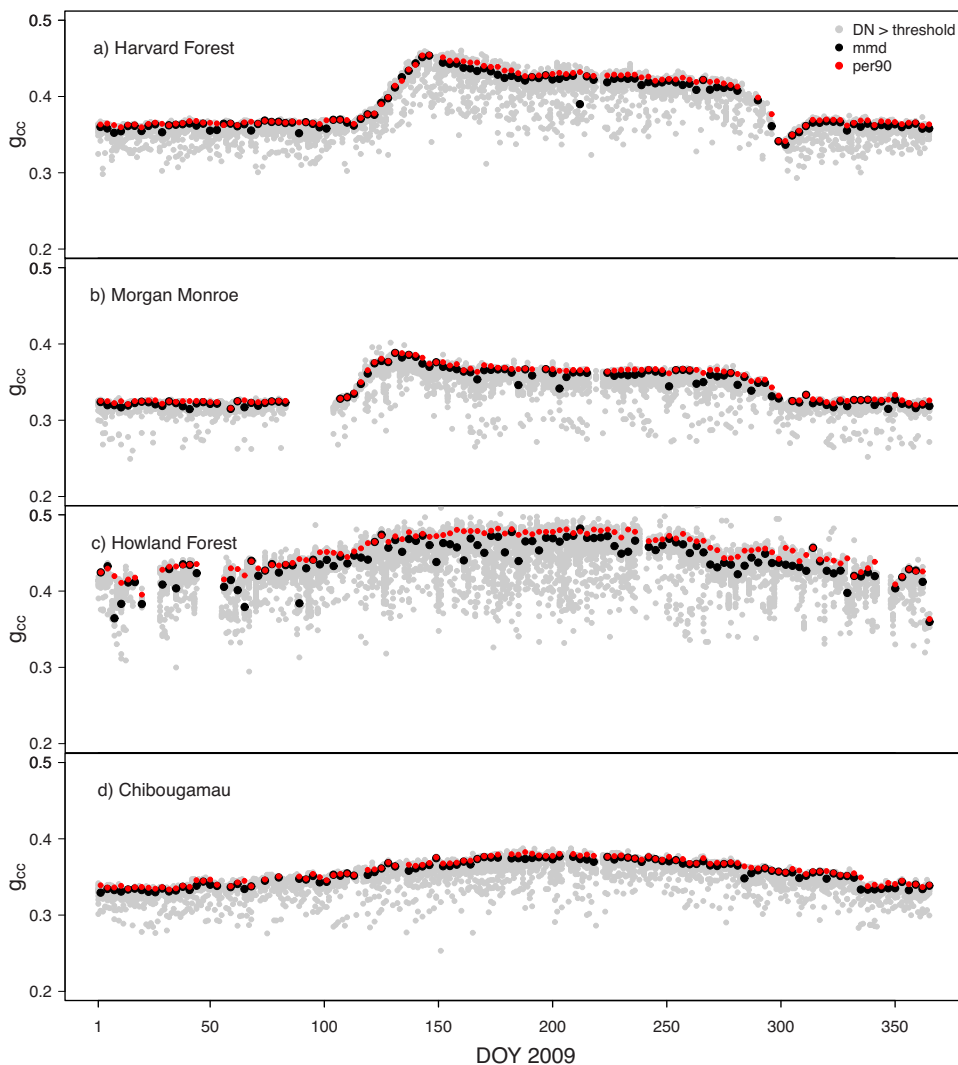
Fig. 6. Three-day green chromatic coordinate (g_{cc}) obtained as mean mid-day values (mmd) and as the 90th percentile of all day-time values within a three-day moving window ($per90$) at two deciduous-dominated forest sites: (a) Harvard Forest and (b) Morgan Monroe State Forest, and at two coniferous-dominated forest sites: (c) Howland Forest and (d) Chibougamou (Table 1). The green chromatic coordinate was filtered for digital camera-specific *RGB* thresholds (digital number (*DN*) > threshold; see Table 3 and text for further explanation). (For interpretation of the references to color in this figure legend, the reader is referred to the web version of the article.)

These measurements will permit calculation of various broadband (albedo, broadband NDVI) and narrowband reflectance indices (NDVI, photochemical reflectance index), as well as f_{APAR}, the fraction of photosynthetically active radiation absorbed by the canopy. The key component of this intercomparison is an automated, multiangular spectroradiometer (AMPSEC II, Hilker et al., 2010), co-mounted on a pan/tilt unit with a StarDot NetCam SC 1.3 MP (Table 2) which is being used in both RGB and RGB-NIR imaging modes. This set up will allow for systematic investigation of several important methodological questions for phenological research based on digital repeat photography such as the role of illumination and viewing geometries and rigorous evaluation of the camera data against calibrated radiometric instruments. Human observer-based assessment of vegetation phenology for trees within the FOV of all instruments will provide a biological context for the observed seasonal changes.

5.1. Scene illumination changes and statistical methodology

Previous studies using image archives spanning from early morning to late evening hours described negligible (Richardson et al., 2009a), symmetrical (Richardson et al., 2009a) or asymmetrical (Ahrends et al., 2008; Sonnentag et al., 2011) diurnal patterns in *RGB* brightness levels due to changes in scene illumination caused by the Earth's daily rotation. In these studies, for each image *RGB* brightness levels were averaged over specified ROIs, To minimize the influence of symmetrical or asymmetrical diurnal patterns in *RGB* brightness levels, *mean* ROI-averaged *RGB* brightness levels from several images over approximately stable mid-day or mid-morning periods (Richardson et al., 2009a; Sonnentag et al., 2011), ROI-averaged *RGB* brightness levels from one representative image from around solar noon (Ahrends et al., 2008, 2009) or ROI-averaged *RGB* brightness levels from several representative images from around solar noon but from different digital cameras of the same model (Kurc and Benton, 2010) were used to obtain daily values of *ExG* or g_{cc}.

Our initial analysis of image archives from Harvard Forest and Howland Forest showed that mid-day averages and one representative image a day caused unwanted variations in daily *ExG* and g_{cc} due to diurnal or weather-related variations in scene illumination (Figs. 3 and 4). Overall we advocate the use of g_{cc}, because their influences in addition to the influence of seasonal changes in scene illumination (Fig. 2) were clearly minimized with g_{cc} compared to
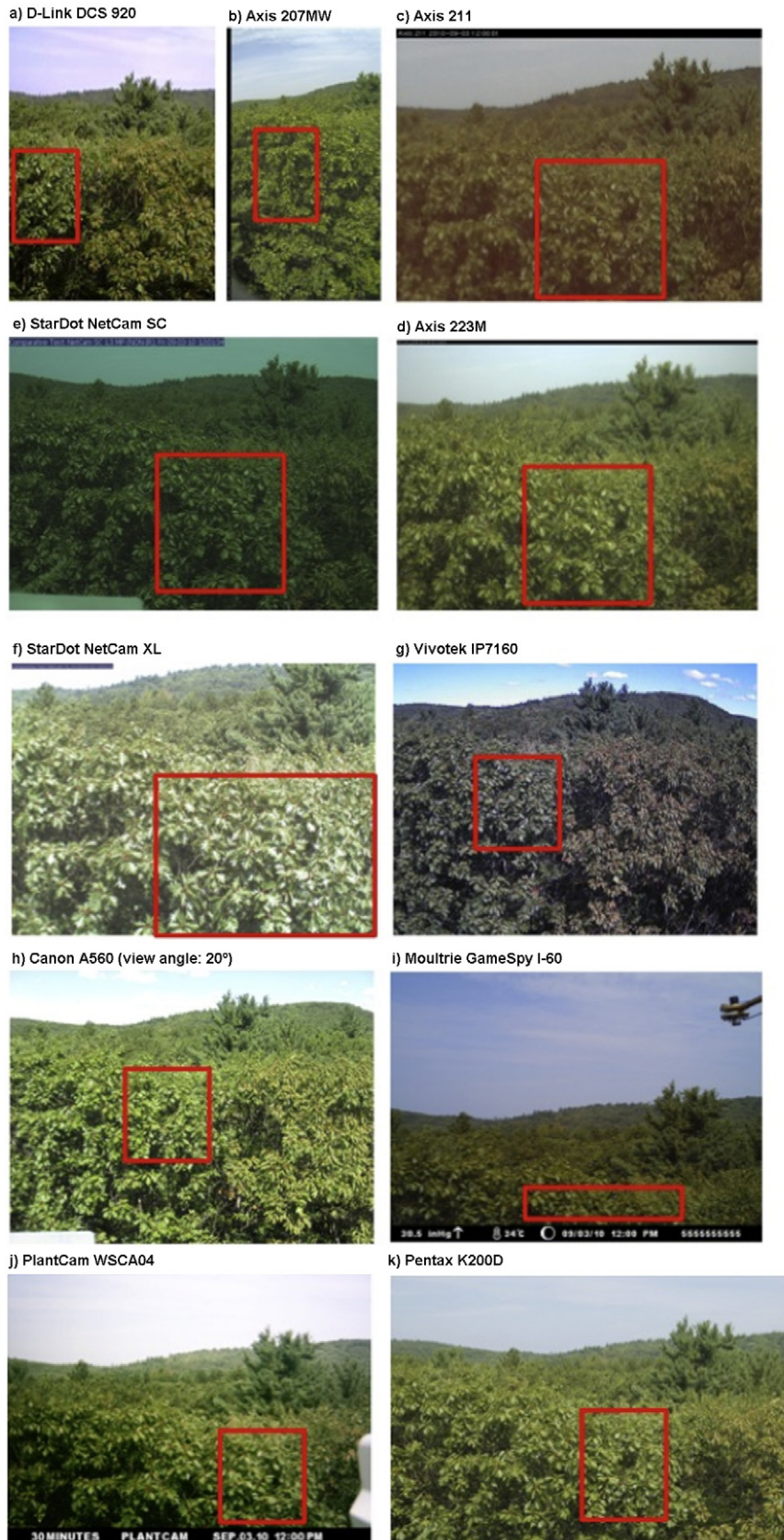
Fig. 7. Example images from Harvard Forest obtained from eleven different digital cameras: (a) D-Link DCS-920 (indoor webcam), (b) Axis 207MW (indoor webcam), (c) Axis 211 (outdoor webcam), (d) Axis 223M (outdoor webcam), (e) StarDot NetCam SC 1.3MP (outdoor webcam), (f) StarDot NetCam XL 3MP (outdoor webcam), (g) Vivotek IP7150 (outdoor webcam), (h) Canon A560 (consumer-grade digital point-and-shoot camera), (i) Moultrie Game Spy I-60 (game-cam), (j) PlantCam WSCA04 (plant-cam), (k) and Pentax K100D (digital single-lens reflex camera; JPEG converted from RAW file with no compression) from around noon (local time) on day-of-year (DOY) 246 in 2010, except for (g) Vivotek IP7160, which is from noon (local time) on DOY 254. The red rectangles are region-of-interests approximately covering the same red oak-dominated portion of the forest canopy. (For interpretation of the references to color in this figure legend, the reader is referred to the web version of the article.)
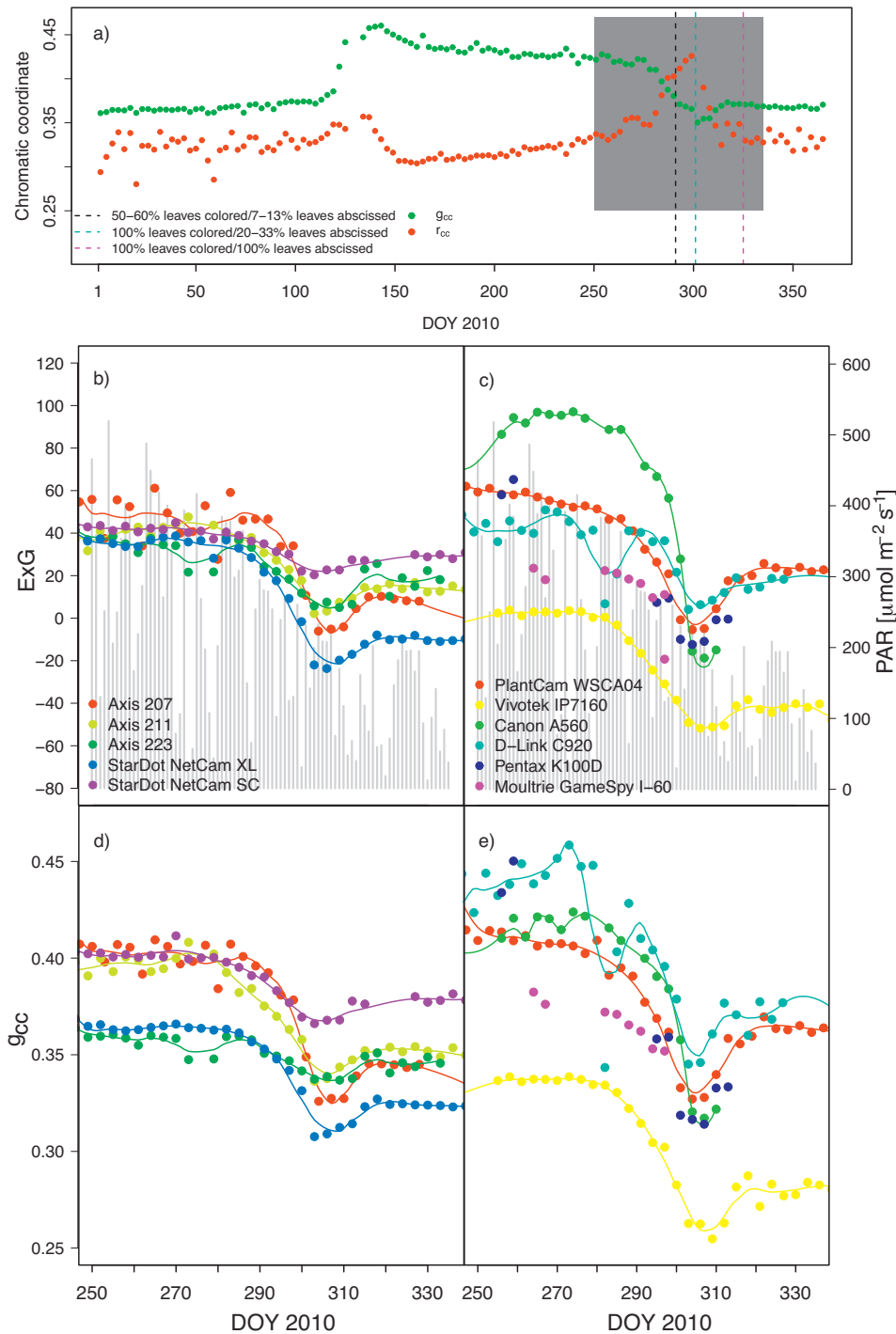
Fig. 8. Three-day (a) green (g_{cc}) and red (r_{cc}) chromatic coordinates at the deciduous-dominated Harvard Forest in 2010 (dark-grey shading indicates the observation period including observer-based estimates of red oak autumn phenology), three-day (b) and (c) *excess green* (*ExG*) and mean daily incoming photosynthetically active radiation (*PAR*) as grey-bar backdrop, and (d) and (e) g_{cc} calculated from *RGB* brightness levels obtained with eleven different digital cameras (Fig. 7) at Harvard Forest (ancillary instrumentation tower). Also included in panels (b)–(e) are daily fitted Loess-curves (span = 0.30) for both *ExG* and g_{cc}. (For interpretation of the references to color in this figure legend, the reader is referred to the web version of the article.)

ExG even though with different success. For example, g_{cc} was more effective in suppressing weather-related variations in scene illumination at Harvard Forest than at Howland Forest, which might be related to color balance differences (Fig. 8) between the StarDot NetCam SC 1.3MP (Harvard Forest) and the older StarDot NetCam XL 1MP (Howland Forest). Ultimately, differences in mean diurnal patterns between overcast and sunny days were still statistically significant in both winter and summer periods (Fig. 4).

The impetus for our moving-window approach, *per90*, was to propose a simple statistical methodology that can be easily implemented and applied to any high-frequency archive of digital landscape images in order to *further* minimize the influence of changes in scene illumination, but at the cost of temporal resolution (daily vs. three-day): the resulting time series of *ExG* or g_{cc} contain a value every third day, which we consider as sufficient for characterizing seasonal canopy development. However, it needs to
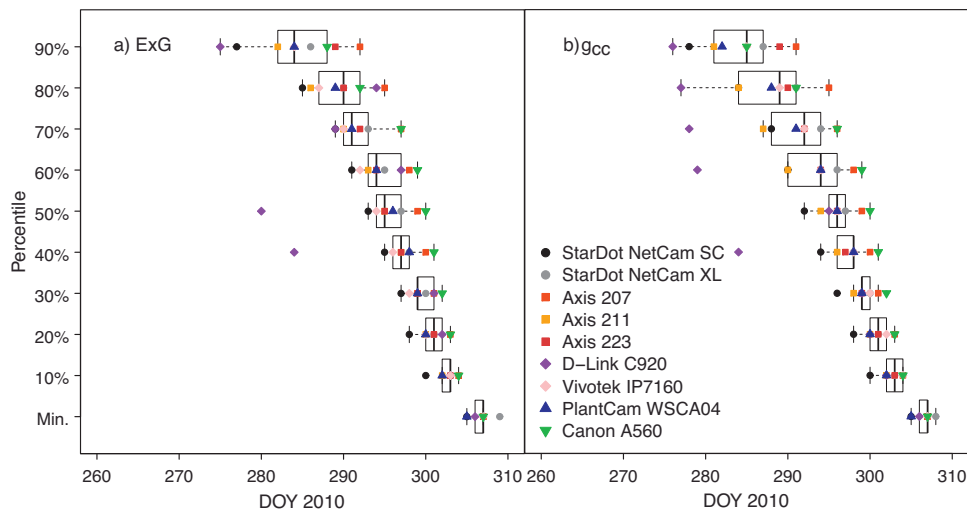
Fig. 9. Comparison of between-digital camera variation in day-of-year (DOY) for complete leaf coloring (i.e., minimum [Min.] canopy greenness) and for different percentiles (10th–90th) of daily Loess curves (span = 0.30) fitted to three-day (a) *excess green* (*ExG*) and (b) the green chromatic coordinate (g_{cc}) obtained as the 90th percentile of all day-time values within a three-day moving window (*per90*). We excluded the Moultrie Game Spy I-60 and the Pentax K100D due to large gaps caused by battery leakage and failure, respectively. (For interpretation of the references to color in this figure legend, the reader is referred to the web version of the article.)

be stressed that the effectiveness of *per90* depends largely on data availability, thus high-frequency image archives are preferred.

5.2. Digital camera and image file format choice

Considering the wide range of imaging sensors (e.g., 1/2.5″-type vs. 1/4″-type CMOS) and imaging sensor technologies (e.g., CMOS vs. CCD) and the seemingly endless combinations of digital camera settings, illumination and viewing geometries, and image file formats, it is a major challenge to successfully intercalibrate or even just to use image archives from different digital cameras for a single purpose. This major challenge makes the direct comparison of *ExG* and g_{cc} from different camera types and models a rather unrealistic endeavour (Fig. 8).

Aside from the differences in absolute values of *ExG* or g_{cc}, the evaluated digital cameras were in good agreement for both *ExG* and g_{cc}, especially with continued canopy coloring toward the end of senescence in late autumn (Fig. 9). The green chromatic coordinate was more effective in suppressing the effects of changes in scene illumination than *ExG* (Figs. 2–4), thus *emphasizing* differences in image quality due to differences in photographic properties and light sensitivities between camera types and models. In contrast, these differences were partly masked by *ExG* since *ExG* is still more influenced by scene illumination than g_{cc}. However, after excluding the most variable vegetation signal from the analysis (i.e., images from the inexpensive indoor webcam D-Link DCS-920), differences between cameras in terms of DOY standard deviations were basically negligible (<0.5 days).

Overall, our results suggest that digital camera choice might be of secondary importance for phenological research when the goal is to identify the timing of key phenological events across sites. For example, the comparison of *ExG* or g_{cc} from different camera types and models appears to be limited regarding more subtle changes in autumn phenology early during senescence such as "50–60% leaves colored/7–13% leaves abscissed" (Fig. 8a) as indicated by wider spreads in DOY between the different cameras at higher percentiles (Fig. 9). In contrast, the better agreement in DOY at lower percentiles and at complete coloring of all leaves (i.e., "100% leaves colored/20–33% leaves abscissed" in Fig. 8a corresponding to the dip in g_{cc}) suggests that key phenological states of the forest canopy as seen by different cameras are comparable. However, it needs to be stressed that differences in how specific cameras "see" the

forest canopy may obscure subtle phenological changes that could be detectable if a common protocol based on one specific camera model was implemented across sites.

Earlier studies comparing different camera types and models for estimating canopy structural parameters based on gap-fraction theory or Beer's Law found that digital camera choice is important, which is not surprising since these efforts, in contrast to ours, require high-quality images to discriminate between fine image details for image binarization (Inoue et al., 2004; Pekin and Macfarlane, 2009). However, in line with findings from these earlier intercomparisons, our results do not suggest that any valuable phenological information is lost in the RAW to JPEG conversion (Fig. 10). Regardless, it needs to be pointed out that in a strict sense unprocessed RAW "is the only scientifically justifiable file format" (Verhoeven, 2010).

Phenological research is largely based on long-term field observations and data sets, ideally spanning several decades or longer (e.g., Menzel et al., 2005; Schleip et al., 2008). Given the advantages of digital repeat photography in terms of logistics, consistency, continuity and objectivity, we expect growing archives of landscape images to become important data streams for phenological research.

One crucial aspect for long-term measurements is the stability of the measured signal. A qualitative first-order approach to assess the stability of the vegetation signal extracted from digital image archives is based on the digital camera signals obtained from invariant grey reference panels in the digital cameras' FOV (Fig. 1).

Visual inspection of reference *RGB* brightness levels, ExG_{ref}, and g_{cc_ref} helps in the interpretation of the obtained vegetation signals and the detection of potential unwanted trends due to imaging sensor degradation that are not related to canopy development. Furthermore, reference *RGB* brightness levels can be used for a simple white balance adjustment: after estimating the maximum reference brightness level (i.e., R_{ref}, G_{ref}, or B_{ref}), the remaining two reference brightness levels are increased by a gain coefficient to obtain the maximum reference brightness levels. Next, these gain coefficients are applied to the original image or the ROI-averaged *RGB* brightness levels (data not shown). However, it needs to be stressed that future efforts should aim for a reference panel positioned *within* the forest canopy and parallel to its top to guarantee that reference panel and forest canopy have similar illumination geometries and are overlooked by the digital cameras at roughly
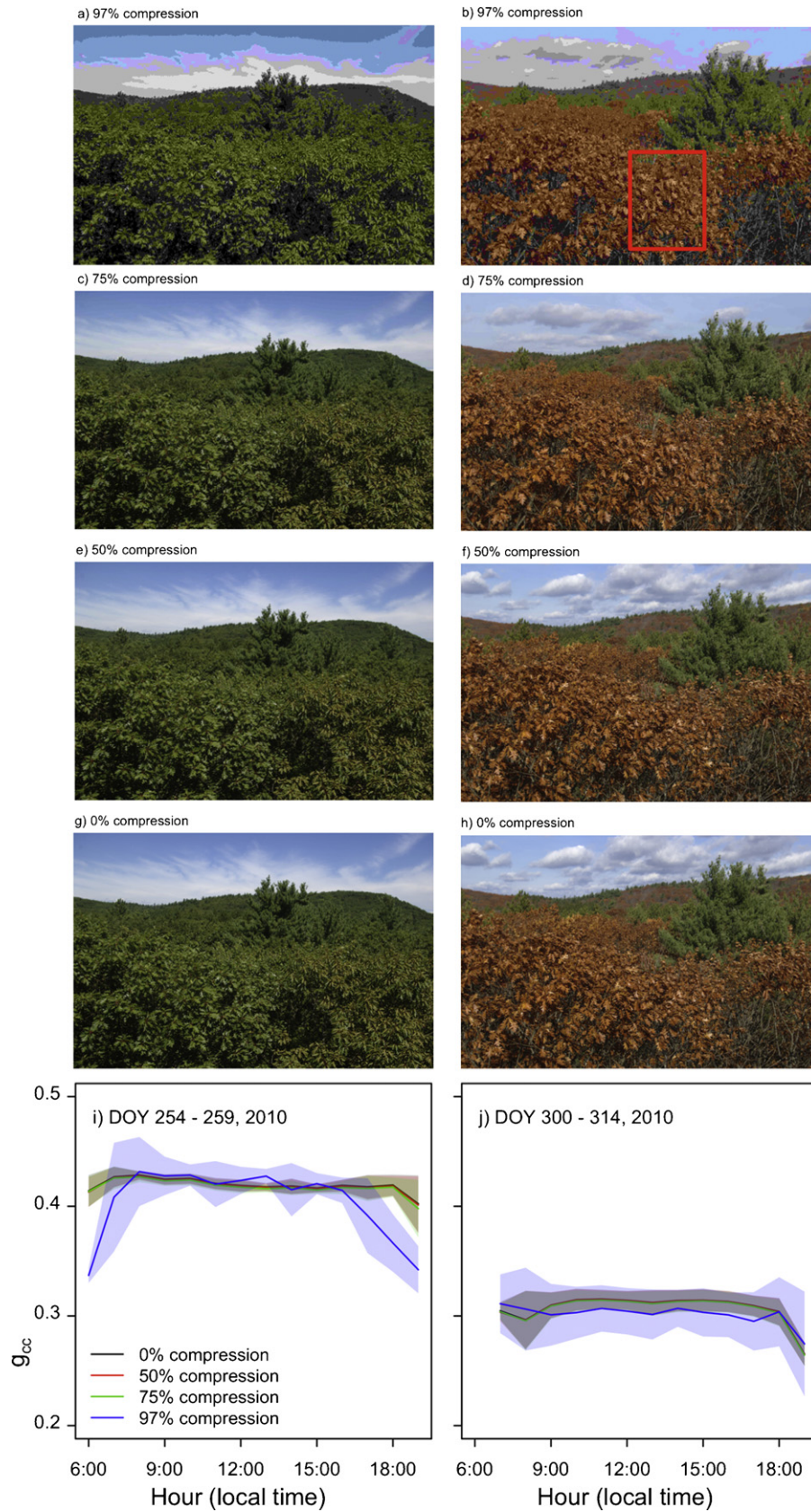
Fig. 10. Effect of different compression rates in the conversion from RAW to 24-bit JPEG files using the Unidentified Flying RAW (UFRAW) utility: no compression during (a) late summer and (b) late autumn, 50% compression during (c) late summer and (d) late autumn, 75% compression during (e) late summer and (f) late autumn, 97% compression during (g) late summer and (h) late autumn, and mean diurnal patterns (±one standard deviation [shaded areas]) of the green chromatic coordinate (g_{cc}) during (i) late summer and (j) late autumn. Note that in panels (i) and (j) the mean diurnal patterns and their standard deviations virtually overlap for 0%, 50% and 75% compression. (For interpretation of the references to color in this figure legend, the reader is referred to the web version of the article.)

the same angle (here: the reference panels at Harvard Forest and Howland Forest were positioned at a tilt angle of roughly 45° facing south directly toward the digital cameras but the canopy tops were more or less horizontal and overlooked at shallow angles). Otherwise, the differences in illumination and viewing geometries between reference panels and vegetation canopies hamper the quantitative use of reference *RGB* brightness levels (e.g., Sonnentag et al., 2011).

In addition, an optimally designed reference panel should probably have several different levels of grey (and not just light-grey causing pixels to saturate easily under well-lit, sunny conditions [Fig. 3]) and also single-color targets, so that the long-term stability of the cameras' imaging sensor can be evaluated in comparison to a identical reference panel kept in the laboratory. Such a reference panel must also be weatherproof, non-fading, and with a smooth but not glossy surface to reduce the build-up of dust and other particulate deposition.

5.3. Digital camera choice from an end-user perspective

Among the numerous options for digital repeat photography, webcams are especially attractive as they are easy to use and to maintain, and their installation and operation requires only minimal to medium-level photographic understanding. The dissemination of growing webcam image archives through the Internet guarantees their easy accessibility. Therefore, webcam image archives constitute a promising data-rich source of phenological information (Graham et al., 2010; Jacobs et al., 2009). Given their nature, webcams can be comfortably configured and maintained remotely through the Internet through a web browser or network protocols such as SSH, minimizing site visits to check upon their proper functioning or to download images. On the downside, webcams have relatively high technical requirements regarding external power supply and Internet connection, especially for their installation in remote areas.

For the purpose of this study we simply distinguished between two broad categories of webcams, "indoor" and "outdoor" (Table 2). The first category includes inexpensive webcams (currently <$100 USD but technologies and costs are changing rapidly) such as the D-Link DCS-920 or the Axis 207MW. Often, their low-resolution digital images are characterized by low sharpness, high noise, low contrast, and poor color balance, partly a result of the limited configuration options regarding photographic properties and light sensitivity. The latter, in particular, might be critical when applying webcams such as the D-Link DCS-920 outdoors under highly varying illumination intensities (Fig. 8c and e). In addition, indoor webcams were not designed for rugged outdoor applications. For example, we had to remove the casing of the D-Link DCS-920 for the digital camera to fit in standard outdoor camera housing (Vitek's VT-EH10). In contrast, all outdoor webcams compared in our study (ranging between around $200 and $1700 USD) were specifically designed for outdoor, (non-scientific) monitoring applications, and most of them provide numerous configuration (and shell scripting options for the StarDot NetCam SC 1.3MP and XL 3MP) options through a web browser interface to configure some important photographic properties and light sensitivity.

In addition to different indoor and outdoor webcams, we also tested a suite of alternative digital camera options that allow for repeat photography, including plant- and game-cams, and P-and-S and DSLR cameras (Fig. 8c and e). The plant-cam and the DLSR camera represent the two opposite ends of the spectrum of digital cameras in Table 2 in terms of photographic understanding and especially costs (PlantCam WSCA04: <$100 USD; Time-Lapse Package [Pentax K100D]: ∼$2600 USD). The PlantCam WSCA04 and the Moultrie Game Spy I-60 (∼$300 USD) offer no

configuration options, whereas the Canon A560 (∼$400 USD) and the Pentax K100D offer numerous options to control photographic properties or light sensitivity typical for modern, state-of-the-art P-and-S and DSLR cameras. Unfortunately, the PlantCam WSCA04 and the Moultrie Game Spy I-60 have to be considered as "black boxes" since the manufacturers declined to release information on the imaging sensors used in these cameras. Images from all four camera types are stored on flash memory cards, thus requiring frequent site visits to retrieve the images and to check upon proper camera functioning. One of the main advantages of the Pentax K100D (or its successor the Canon Rebel XS 1000D) as part of Harbortronic's Time-Lapse Package is the autonomous design in a rugged outdoor camera housing with a solar panel that allows its installation in remote areas (Bater et al., 2011). In contrast, the PlantCam WSCA04, the Moultrie Game Spy I-60 and the Canon A560 are operated on batteries, whereas the latter two can optionally be operated on external DC power.

Our intercomparison of different digital repeat photography options for phenological research did not reveal any major influence of digital camera choice on *ExG* and g_{cc}, except for inexpensive indoor webcams such as the D-Link DCS-920 (Fig. 9). In addition, our findings suggest that even image archives in JPEG format derived from inexpensive "black boxes", such as the PlantCam WSCA04, are sufficient to characterize canopy development for phenological research.

6. Conclusions

In this study we analyzed one-year image archives from Harvard Forest and Howland Forest to examine how diurnal, seasonal and weather-related changes in scene illumination affect *excess green*, *ExG*, and the green chromatic coordinate, g_{cc}. Both descriptors of canopy greenness failed to entirely remove these effects, but g_{cc} was generally more effective than *ExG* in suppressing them. To further minimize the effects of scene illumination changes, we propose to calculate three-day g_{cc} using a moving-window approach, *per90*, that assigns the 90th percentile of all day-time values to the window center day.

Through intercomparison of multi-month image archives obtained with eleven different digital cameras we found that digital camera choice might be of secondary importance despite large differences in the absolute values of *ExG* and g_{cc}. Our results do not suggest that any phenologically relevant information is lost in the conversion from RAW to JPEG format, the most common image file format standard. Based on this study and the experiences made with different digital camera types and models, we recommend

(i) The use of g_{cc} in combination with *per90* as a means to characterize the temporal development of forest canopies based on high-frequency digital landscape image archives (e.g., images taken at 30-min intervals during daytime).

(ii) The use of outdoor webcams (e.g., StarDot, Axis or Vivotek) for monitoring of vegetation status with g_{cc} given the appropriate infrastructure (pre-requisites: minimal to medium-level photographic understanding).

(iii) The use of simple "black boxes" such as plant-cams for monitoring of vegetation status with g_{cc} at remote locations lacking appropriate infrastructure (no pre-requisites regarding photographic understanding).

(iv) The installation of reference panels with different levels of grey and/or single-color targets in the digital cameras' FOV (ideally within the forest canopy) to provide a first-order means to assess the continuity and stability of g_{cc} over time.

Acknowledgements

References

Adamsen, F.J., Coffelt, T.A., Nelson, J.M., Barnes, E.M., Rice, R.C., 2000. Method for using images from a color digital camera to estimate flower number. Crop Sci. 40, 704–709.

Adamsen, F.J., Pinter, P.J., Barnes, E.M., LaMorte, R.L., Wall, G.W., Leavitt, S.W., Kimball, B.A., 1999. Measuring wheat senescence with a digital camera. Crop Sci. 39, 719–724.

Ahrends, H.E., Brugger, R., Stockli, R., Schenk, J., Michna, P., Jeanneret, F., Wanner, H., Eugster, W., 2008. Quantitative phenological observations of a mixed beech forest in northern Switzerland with digital photography. J. Geophys. Res.: Biogeogr., doi:10.1016/j.agrformet.2011.02.011.

Ahrends, H.E., Etzold, S., Kutsch, W.L., Stoeckli, R., Bruegger, R., Jeanneret, F., Wanner, H., Buchmann, N., Eugster, W., 2009. Tree phenology and carbon dioxide fluxes: use of digital photography at for process-based interpretation the ecosystem scale. Clim. Res. 39, 261–274.

Bater, C.W., Coops, N.C., Wulder, M.A., Hilker, T., Nielsen, S.E., McDermid, G., Stenhouse, G.B., 2011. Using digital time-lapse cameras to monitor species understorey and overstorey phenology in support of wildlife habitat assessment. Environ. Monit. Assess., doi:10.1007/s10661-010-1768-x.

Bergeron, O., Margolis, H.A., Black, T.A., Coursolle, C., Dunn, A.L., Barr, A.G., Wofsy, S.C., 2007. Comparison of carbon dioxide fluxes over three boreal black spruce forests in Canada. Glob. Change Biol. 13, 89–107.

Cheng, H.D., Jiang, X.H., Sun, Y., Wang, J.L., 2001. Color image segmentation: advances and prospects. Pattern Recogn. 34, 2259–2281.

Cleveland, W.S., 1979. Robust locally weighted regression and smoothing scatterplots. J. Am. Stat. Assoc. 74, 829–836.

Cleveland, W.S., Devlin, S.J., 1988. Locally weighted regression – an approach to regression analysis by local fitting. J. Am. Stat. Assoc. 83, 596–610.

Ensminger, I., Sveshnikov, D., Campbell, D.A., Funk, C., Jansson, S., Lloyd, J., Shibistova, O., Öquist, G., 2004. Intermittent low tempereatures constrain spring recovery of photosynthesis in boreal Scots pine forests. Glob. Change Biol. 10, 995–1008.

Garrity, S.R., Vierling, L.A., Bickford, K., 2010. A simple filtered photodiode instrument for continuous measurement of narrowband NDVI and PRI over vegetated canopies. Agric. Forest Meteorol. 150, 489–496.

Gillespie, A.R., Kahle, A.B., Walker, R.E., 1987. Color enhancement of highly correlated images. 2. Channel ratio and chromaticity transformation techniques. Remote Sens. Environ. 22, 343–365.

Graham, E.A., Riordan, E.C., Yuen, E.M., Estrin, D., Rundel, P.W., 2010. Public Internet-connected cameras used as a cross-continental ground-based plant phenology monitoring system. Glob. Change Biol. 16, 3014–3023.

Hilker, T., Nesic, Z., Coops, N.C., Lessard, D., 2010. A new, automated, multiangular radiometer instrument for tower-based observations of canopy reflectance (AMPEC II). Instrum. Sci. Technol. 261, 1467–1478.

Hollinger, D.Y., Aber, J., Dail, B., Davidson, E.A., Goltz, S.M., Hughes, H., Leclerc, M.Y., Lee, J.T., Richardson, A.D., Rodrigues, C., Scott, N.A., Achuatavarier, D., Walsh, J., 2004. Spatial and temporal variability in forest-atmosphere CO_2 exchange. Glob. Change Biol. 10, 1689–1706.

Ide, R., Oguma, H., 2010. Use of digital cameras for phenological observations. Ecol. Inform. 5, 339–347.

Inoue, A., Yamamoto, K., Mizoue, N., Kawahara, Y., 2004. Effects of image quality, size and camera type on forest light environment estimates using digital hemispherical photography. Agric. Forest Meteorol. 126, 89–97.

Jacobs, N., Burgin, W., Fridrich, N., Abrams, A., Miskell, K., Braswell, B.H., Richardson, A.D., Pless, R., 2009. The global network of outdoor webcams: properties and applications. In: Proceedings ACM GIS'09, Seattle, WA, USA, November 4–6, pp. 111–120.

Kurc, S.A., Benton, L.M., 2010. Digital image-derived greenness links deep soil moisture to carbon uptake in a creosotebush-dominated shrubland. J. Arid Environ. 74, 585–594.

Menzel, A., Estrella, E., Testka, A., 2005. Temperature response rates from long-term phenological records. Clim. Res. 30, 21–28.

Meyer, G.E., Neto, J.C., 2008. Verification of color vegetation indices for automated crop imaging applications. Comput. Electron. Agric. 63, 282–293.

Migliavacca, M., Galvagno, M., Cremonese, E., Rossini, M., Meroni, M., Sonnentag, O., Manca, G., Diotri, F., Busetto, L., Cescatti, A., Colombo, R., Fava, F., Morra di Cella, U., Pari, E., Siniscalco, C., Richardson, A., 2011. Using digital repeat photography and eddy covariance data to model grassland phenology and photosynthetic CO_2 uptake. Agric. Forest Meteorol. 151, 1325–1337.

Monson, R.K., Turnipseed, A.A., Sparks, J.P., Harley, P.C., Scott-Denton, L.E., Sparks, K., Huxman, T.E., 2002. Carbon sequestration in a high-elevation, subalpine forest. Glob. Change Biol. 8, 459–478.

Morisette, J.T., Richardson, A.D., Knapp, A.K., Fisher, J.I., Graham, E.A., Abatzoglou, J., Wilson, B.E., Breshears, D.D., Henebry, G.M., Hanes, J.M., Liang, L., 2009. Tracking the rhythm of the seasons in the face of global change: phenological research in the 21st century. Front. Ecol. Environ. 7, 253–260.

Pekin, B., Macfarlane, C., 2009. Measurement of crown cover and leaf area index using digital cover photography and its application to remote sensing. Remote Sens. 1, 1298–1320.

Perez, A.J., Lopez, F., Benlloch, J.V., Christensen, S., 2000. Colour and shape analysis techniques for weed detection in cereal fields. Comput. Electron. Agric. 25, 197–212.

Richardson, A.D., Bailey, A.S., Denny, E.G., Martin, C.W., O'Keefe, J., 2006. Phenology of a northern hardwood forest canopy. Glob. Change Biol. 12, 1174–1188.

Richardson, A.D., Braswell, B.H., Hollinger, D.Y., Jenkins, J.P., Ollinger, S.V., 2009a. Near-surface remote sensing of spatial and temporal variation in canopy phenology. Ecol. Appl. 19, 1417–1428.

Richardson, A.D., Hollinger, D.Y., Dail, D.B., Lee, J.T., Munger, J.W., O'Keefe, J., 2009b. Influence of spring phenology on seasonal and annual carbon balance in two contrasting New England forests. Tree Physiol. 29, 321–331.

Richardson, A.D., Jenkins, J.P., Braswell, B.H., Hollinger, D.Y., Ollinger, S.V., Smith, M.L., 2007. Use of digital webcam images to track spring green-up in a deciduous broadleaf forest. Oecologia 152, 323–334.

Richardson, A.D., O'Keefe, J., 2009. Phenological differences between understory and overstory: a case study using the long-term Harvard Forest records. In: Noormets, A. (Ed.), Phenology of ecosystem processes. Springer, New York, NY, pp. 87–117.

Ryu, Y., Baldocchi, D.D., Verfaillie, J., Ma, S., Falk, M., Ruiz-Mercado, I., Hehn, T., Sonnentag, O., 2010. Testing the performance of a novel spectral reflectance sensor, built with light emitting diodes (LEDs), to monitor ecosystem metabolism, structure and function. Agric. Forest Meteorol. 150, 1597–1606.

Schleip, C., Rutishauser, T., Luterbacher, J., Menzel, A., 2008. Time series modeling and central European temperature impact assessment of phenological records over the last 250 years. J. Geophys. Res.: Biogeogr., doi:10.1029/2007JG000646.

Schmid, H.P., Grimmond, C.S.B., Cropley, F., Offerle, B., Su, H.B., 2000. Measurements of CO_2 and energy fluxes over a mixed hardwood forest in the mid-western United States. Agric. Forest Meteorol. 103, 357–374.

Sonnentag, O., Detto, M., Vargas, R., Ryu, Y., Runkle, B.R.K., Kelly, M., Baldocchi, D.D., 2011. Tracking the structural and functional development of a perennial pepperweed (Lepidium latifolium L.) infestation using a multi-year archive of webcam imagery and eddy covariance measurements. Agric. Forest Meteorol. 151, 916–926.

Tucker, C.J., 1979. Red and photographic infrared linear combinations for monitoring vegetation. Remote Sens. Environ. 8, 127–150.

Urbanski, S., Barford, C., Wofsy, S., Kucharik, C., Pyle, E., Budney, J., McKain, K., Fitzjarrald, D., Czikowsky, M., Munger, J.W., 2007. Factors controlling CO_2 exchange on timescales from hourly to decadal at Harvard Forest. J. Geophys. Res.: Biogeogr., doi:10.1029/2006JG000293.

Verhoeven, G.J.J., 2010. It's all about the format – unleashing the power of RAW aerial photography. Int. J. Remote Sens. 31, 2009–2042.

Woebbecke, D.M., Meyer, G.E., Vonbargen, K., Mortensen, D.A., 1995. Color indexes for weed identification under various soil, residue, and lighting conditions. Trans. ASAE 38, 259–269.